Economic Geology, v. 120, no. 4, pp. 903–924

The 3.53 Ga St. James Volcanogenic Massive Sulfide Deposit, Kaapvaal Craton: Links to Submarine Rhyolites, Not to Komatiites

T. Netshidzivhe,[1,2,†] S. Tappe,[1,3,†] A. H. Wilson,[4] S. Burness,[1,5] J. F. Wotzlaw,[6] H. Strauss,[7] K. A. Smart,[3,4] B. M. Guy,[1,8] and K. S. Viljoen[1]

[1]*Department of Geology, University of Johannesburg, Auckland Park 2006, South Africa*

[2]*Unit for Environmental Sciences and Management, Geology, North-West University, Potchefstroom 2531, South Africa*

[3]*Institute for Mineralogy, Technical University Bergakademie Freiberg, 09599 Freiberg, Germany*

[4]*School of Geosciences, University of the Witwatersrand, Johannesburg 2050, South Africa*

[5]*Department of Chemical Engineering, University of Cape Town, Rondebosch 7701, South Africa*

[6]*Department of Earth Sciences, ETH Zürich, Zürich, Switzerland*

[7]*Institute for Geology and Paleontology, University of Münster, 48149 Münster, Germany*

[8]*Helmholtz-Zentrum Dresden-Rossendorf, Helmholtz Institute Freiberg for Resource Technology, 09599 Freiberg, Germany*

Abstract

The Nondweni greenstone belt is located in the southeastern region of the Kaapvaal craton in South Africa and contains significant volumes of 3.53 to 3.45 Ga mafic-ultramafic lava flows (komatiitic and tholeiitic basalts). Minor felsic volcanic rock units, such as massive rhyolites and deformed quartz-feldspar-mica schists (felsic schists), also occur and are demonstrably linked to small base metal sulfide orebodies, interpreted here as volcanogenic massive sulfide (VMS)-type mineralization (e.g., sphalerite, chalcopyrite, pyrrhotite, pyrite, galena, acanthite). Chemical abrasion-isotope dilution-thermal ionization mass spectrometry (CA-ID-TIMS) U-Pb zircon analysis yields a rhyolite eruption age of 3531.91 ± 0.46 Ma for the felsic volcanic rock unit that hosts VMS-type mineralization at the St. James deposit, which renders this Zn-Cu-Pb-Ag mineralization among the oldest preserved of its kind, offering insights into ore-forming processes that took place on and below the Paleoarchean sea floor. Rare earth element geochemical modeling suggests that the felsic volcanic rocks formed by moderate degrees of partial melting of hydrothermally altered basalts similar in composition to those from the Nondweni greenstone belt. Regarding ore formation, we envisage a scenario where basaltic ocean floor, in close proximity to a back-arc spreading ridge, had been intensively altered and subjected to elevated temperatures, which facilitated localized melting at low pressures (<2 kbar), resulting in the production of rhyolitic magmas accompanied by hydrothermal sulfide deposition. This model is supported by evidence from multiple sulfur isotope data ($\delta^{34}S$ and $\Delta^{33}S$), which demonstrates that the basaltic rocks contain unfractionated magmatic sulfur and the rhyolitic rocks contain sulfur sourced from altered oceanic basalts. In contrast, the rhyolite-associated VMS-type mineralization records even more complex sulfur interactions, including contributions from surficial mass-independent fractionated sulfur isotopic components; that is, these base metal sulfide ores exhibit a negative sulfur mass-independent fractionation signature of –0.53‰ $\Delta^{33}S$.

Introduction

Volcanogenic massive sulfide (VMS) mineralization deposits are among the oldest ore deposits recorded on Earth and provide a significant resource of Cu, Zn, Pb, Au, and Ag, hosted primarily within chalcopyrite, sphalerite, galena, and other base metal sulfides (Franklin et al., 1981; Lydon, 1984; Ohmoto, 1996; Franklin et al., 2005; Hannington, 2014). These sulfide mineral deposits precipitate from hot hydrothermal fluids (250°–400°C) and are commonly associated with mafic-ultramafic but also felsic rocks on the sea floor (Franklin et al., 1981, 2005; Huston et al., 2010; Hannington, 2014). They occur typically within extensional tectonic settings such as mid-ocean ridges and back-arc basins, but also near volcanic arcs (e.g., Schwarz-Schampera et al., 2010).

The geologic record suggests that VMS deposit formation was frequent during the Neoarchean, Paleoproterozoic, and Phanerozoic, including modern analogs in the form of seafloor massive sulfides. The Superior, Slave, and Yilgarn cratons account for over 90% of the recorded Archean VMS deposits, with >115 VMS deposits known from the Superior craton in Canada (Mercier-Langevin et al., 2011). Some of the oldest known VMS deposits occur on the Pilbara craton as part of the ca. 3481 Ma Dresser barite deposit as well as the 3474 to 3459 Ma Duffer Formation (Huston et al., 2007; Hickman and Van Kranendonk, 2008; Van Kranendonk et al., 2008). Archean greenstone belts that host VMS deposits

†Corresponding authors: email, Thendo.Netshidzivhe@nwu.ac.za; sebastian.tappe@mineral.tu-freiberg.de

© 2025 Gold Open Access: This paper is published under the terms of the CC-BY-NC license.

ISSN 0361-0128; doi:10.5382/econgeo.5162; 22 p.
Digital appendices are available in the online Supplements section.

Submitted: March 20, 2024 / Accepted: March 2, 2025

Downloaded from http://pubs.geoscienceworld.org/segweb/economicgeology/article-pdf/120/4/903/7306681/5162_netshidzivhe_et_al.pdf
by The Lib. East China Geol Inst. user

are commonly associated with a specific suite of rocks (e.g., Lesher et al., 1986). This allows for the deposits to be classified on the basis of the host lithostratigraphy, as well as the inferred geodynamic setting and petrogenetic affinity (e.g., Lentz, 1998; Barrie and Hannington, 1999; Franklin et al., 2005; Galley et al., 2007). The host lithostratigraphy can be grouped into one or more of the following: (1) mafic, (2) mafic-siliciclastic, (3) bimodal-mafic, (4) bimodal-felsic, and (5) felsic-siliciclastic (or bimodal-siliciclastic). The first three groups are dominated by mafic rocks associated with siliciclastic and chemical sedimentary rocks, with a minor felsic rock component. A common characteristic of these three groups is their juvenile nature, with very little involvement of continental crustal components. In contrast, groups 4 and 5 are dominated by felsic and sedimentary rock successions (Barrie and Hannington, 1999).

The sources of base metals that contributed to the accumulation of ore deposits on the Archean sea floor remain a subject of debate. The formation of some VMS deposits has been attributed to hydrothermal circulation through the oceanic crust, where metals and sulfur are leached from the volcanic rocks at ~350°C (Alt, 1994, 1995; Nielsen et al., 2006; Patten et al., 2016). A direct contribution of metals and sulfur from magmatic fluids has also been suggested (Nadeau et al., 2010; Kalender, 2011; Mungall et al., 2015; Virtanen et al., 2021). Archean VMS deposits share many similarities with modern-day VMS deposits in terms of their geometry, mineralization, and alteration styles (Mercier-Langevin et al., 2014). These similarities have been used to infer that the VMS ore-forming processes have remained essentially unchanged since the Archean.

This study explores the Paleoarchean Nondweni greenstone belt, which is host to a relatively small base metal sulfide mineralization associated with metavolcanic rocks (the so-called St. James deposit). The Nondweni greenstone belt is located ~200 km south of the archetypal Barberton greenstone belt on the Kaapvaal craton (App. Fig. A1). According to Wilson and Versfeld (1994a), the main base metal occurrence at Nondweni is hosted by a quartz-feldspar-mica schist (felsic schist), with an apparent structural control in fold closures (Figs. 1–2). The mineralization is dominated by sphalerite, pyrrhotite, and chalcopyrite, with lesser pyrite and galena. Other small Archean VMS deposits on the Kaapvaal craton have been reported from the Barberton and Murchison greenstone belts (Schwarz-Schampera et al., 2010).

The VMS mineralization in the Nondweni greenstone belt provides an opportunity to investigate possible relationships between volcanism and sea-floor metallogenesis on the early Earth. For other VMS deposits, detailed geochemical studies of volcanic rocks have long been used to investigate the potential of volcanic activity as heat sources that drive hydrothermal circulation (Spooner and Fyfe, 1973; Campbell et al., 1981; Franklin et al., 1981; Galley, 1993, 2003; Cathles et al., 1997). For the approximately 3.5- to 3.4-b.y.-old Nondweni greenstone belt, the wide range of metavolcanic rock types is particularly insightful for exploring the tectonomagmatic environment and the conditions that led to massive sea-floor mineralization. We report whole-rock major and trace element data for both ultramafic-mafic and felsic metavolcanic assemblages to constrain the petrogenesis and geologic setting of the Paleoarchean igneous activity in the Nondweni greenstone belt. These geochemical data are complemented by new U-Pb zircon and monazite age determinations of the immediate rhyolitic host rocks to the VMS mineralization to understand the timing of magma emplacement, sea-floor mineralization, and low-grade greenschist facies metamorphism of the volcanosedimentary succession in this sparsely investigated region of the Kaapvaal craton. Our new age determinations suggest that the St. James occurrence is the oldest preserved VMS deposit in the world. In addition, a textural study of the sulfide ore mineral assemblage is carried out to enable classification of the mineralization. The first major and minor element compositional data for the sulfides enable us to place constraints on the ore-forming processes at Nondweni. Bulk sulfide ore and volcanic rock multiple sulfur isotope compositions ($\delta^{34}S$ and $\Delta^{33}S$) are used as important tracers of sulfur provenance in this understudied Paleoarchean VMS-style mineralized district.

Geology of the Nondweni Greenstone Belt

The Paleoarchean volcanosedimentary succession of the Nondweni greenstone belt in South Africa forms a series of inliers distributed between the Barberton greenstone belt in the north and the southern margin of the Kaapvaal craton (Versfeld and Wilson, 1992; Hofmann et al., 2019). It is named after the Nondweni River, which transgresses the greenstone belt and is located approximately 200 km south of the Barberton greenstone belt (App. Fig. A1). The ~18-km-wide belt of supracrustal rocks in this area is collectively known as the Nondweni Group, extending ~30 km in a north-south direction and covering an area of 270 km^2 (Versfeld, 1988; Wilson and Riganti, 2022). The Nondweni Group is subdivided lithostratigraphically into three formations: the Toggekry Formation (ca. 3.5 Ga), the Magongolozi Formation (ca. 3.4 Ga), and the Witkop Formation (ca. 3.4 Ga; Tarduno et al., 2010; Xie et al., 2012). The entire succession forms a NE- to SW-trending synclinal structure resulting from steep isoclinal folding (Fig. 1). The eastern boundary of the greenstone belt is marked by an intrusive contact with the ca. 3.29 Ga Mvunyana granodiorite (Matthews et al., 1989). The three formations of the Nondweni Group are described below.

The Toggekry Formation is a steeply dipping, E-W–trending succession, which measures ~2,000 m in thickness (Versfeld and Wilson, 1992). It is exposed in the northeastern portion of the belt and is characterized by a bimodal succession of felsic metavolcanic rocks (massive rhyolites and quartz-feldspar-sericite schists) intercalated with subordinate mafic and ultramafic metavolcanic rocks. The rocks of the Toggekry Formation have experienced the bulk of deformation within the Nondweni greenstone belt, mainly because of their location in the hinge zone of the synclinal fold closure and proximity to the Mesoarchean granitoids in the east (Hofmann and Wilson, 2007). The Toggekry Formation contains several small massive sulfide occurrences dominated by sphalerite, chalcopyrite, and pyrrhotite (Fig. 2). The southern boundary of the Toggekry Formation coincides with cessation of the felsic volcanism (Riganti and Wilson, 1995).

The Magongolozi Formation (~7,000 m thick; Wilson and Versfeld, 1992a) is exposed in the northwestern part of the

Downloaded from http://pubs.geoscienceworld.org/segweb/economicgeology/article-pdf/120/4/903/7306681/5162_netshidzivhe_et_al.pdf
by The Lib. East China Geol Inst. user

Nondweni greenstone belt over a strike length of ~13 km. This formation is dominated by pillowed metabasalts, coarse pyroxene spinifex-textured mafic and ultramafic rocks, as well as intermediate metavolcanic rocks that are interlayered with subordinate chert and quartzite (Wilson and Carlson, 1989). The Magongolozi Formation is intruded by ca. 2.9 Ga mafic sills of gabbroic and dioritic compositions (Versfeld, 1988).

The Witkop Formation is preserved at both limbs of the large-scale synclinal structure (Wilson and Versfeld, 1992b). This ~7,500-m-thick succession is dominated by more primitive metavolcanic rocks compared to the other two formations. The Witkop Formation is characterized by komatiitic basalts and pillowed basalts, which are intercalated with subordinate banded cherts. The top of the Witkop Formation is marked

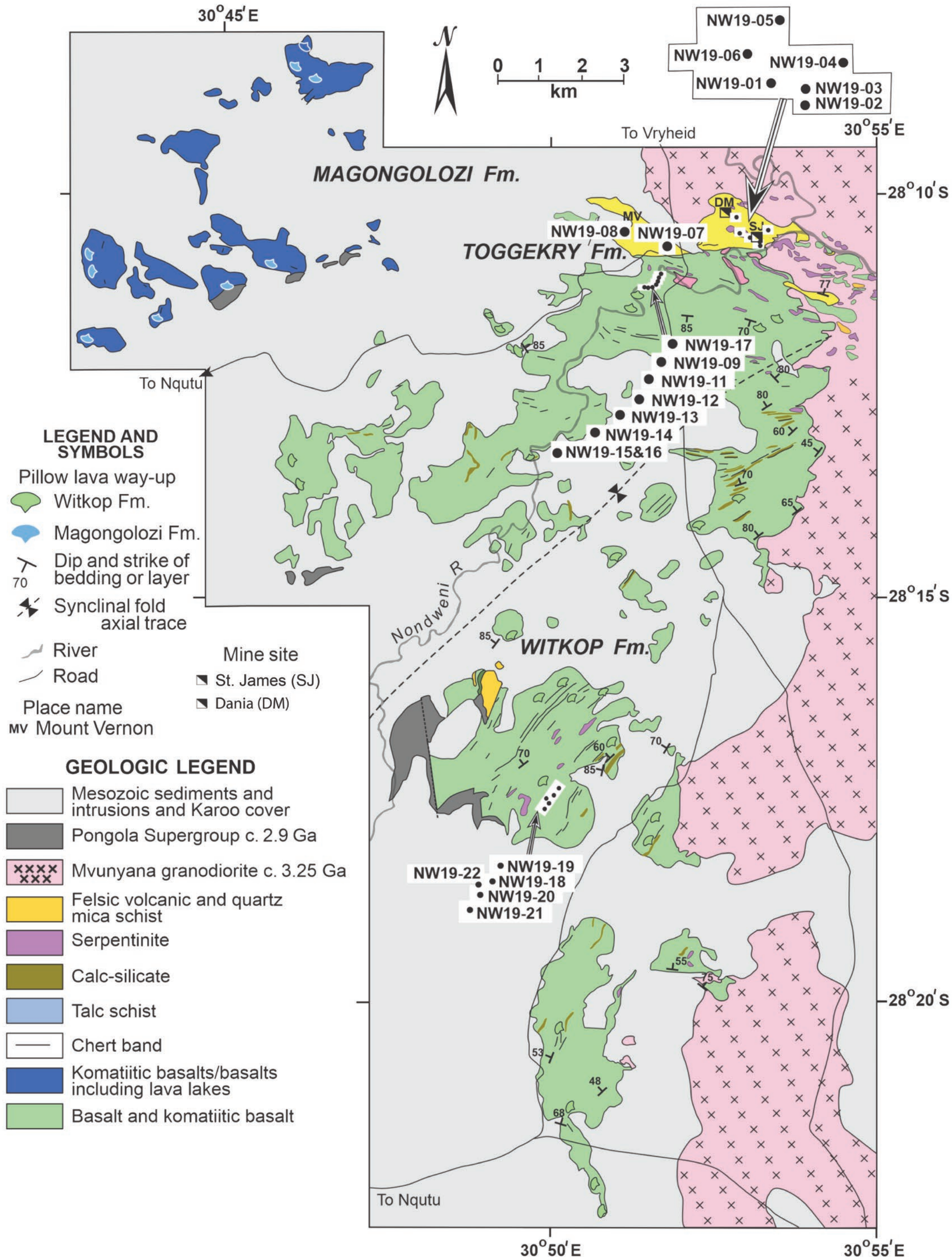

Fig. 1. Simplified geologic map of the Nondweni greenstone belt modified after Wilson and Riganti (2022). Sample sites and sample numbers (NW19) for this study are shown in the expanded layouts and relate to actual positions on the map indicated by the bold arrows.

Downloaded from http://pubs.geoscienceworld.org/segweb/economicgeology/article-pdf/120/4/903/7306681/5162_netshidzivhe_et_al.pdf
by The Lib. East China Geol Inst. user

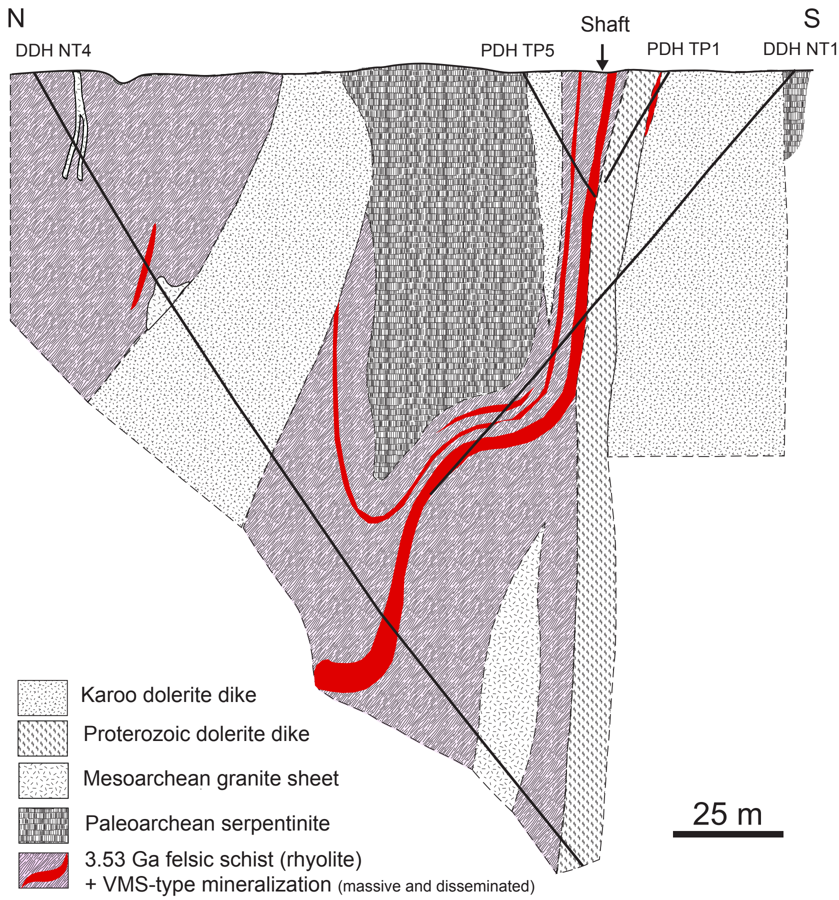

Fig. 2. Interpretative geologic cross section of the St. James volcanogenic massive sulfide (VMS)-style mineralization in the Nondweni greenstone belt, South Africa. The cross section is redrawn from Versfeld (1988), using combined information from surface mapping and four exploration boreholes shown as black lines. The serpentinite body and 3.53 Ga felsic schist unit are part of the Paleoarchean Toggekry Formation, which is host to the stratiform base metal sulfide orebodies in the Nondweni Group.

by a ~500-m-thick sedimentary rock succession comprising conglomerates, sandstones, and cherts (Wilson and Versfeld, 1994b). Beneath the chert horizon occurs a 20- to 50-m-thick alteration zone that is characterized by extremely high SiO_2 contents (~90 wt %) and variable K_2O, Rb, and Ba compositions. Hofmann and Wilson (2007) concluded that this zone is the result of syndepositional sea-floor hydrothermal processes at temperatures of <150°C. Such intercalations of mafic-ultramafic metavolcanic rocks and relatively thin chert horizons are also reported from the lowermost stratigraphic sections of the Paleoarchean Barberton greenstone belt (de Wit et al., 2011; Hofmann et al., 2013).

The St. James VMS deposit

Knowledge about the sulfide orebodies at the St. James prospect is derived from four inclined borehole intersections, a 43-m-deep shaft, and a decline. These advanced exploration activities were carried out intermittently by several companies between the 1910s and 1980s (e.g., Iscor, Somerset Mining, Anglo American, African Selection Trust Exploration). The mode of occurrence of the St. James base metal sulfide mineralization is illustrated in an interpretive geologic cross section (Fig. 2, modified after Versfeld, 1988) and can be described as follows.

The ore is hosted by quartz-feldspar-mica (felsic) schists of the Toggekry Formation and occurs as stringers, pods, and lenses of massive sulfide typically concentrated in fold closure zones of a steeply plunging, larger-scale structure. The folded felsic schist unit envelops a sizeable, more competent serpentinite body and is characterized by a gossan at the surface. The Paleoarchean schists and serpentinites are intruded by Mesoarchean granite dikes and also by dolerite dikes of Proterozoic and Mesozoic ages (e.g., Karoo dikes). The discontinuous sulfide ore stringers within the felsic schists are up to 5 m thick and appear to be bedded, as well as mineralogically zoned (e.g., Zn-rich tops and Cu-rich bottoms). They are concordantly aligned with the main foliation plane of the isoclinally folded felsic schists. Although the Zn and Cu (and Ag) grades are elevated in several drill core intersections, the various drilling campaigns delineated only subeconomic tonnages of base metal sulfide ore.

Sampling of representative lithologies in the Nondweni greenstone belt

Twenty-nine samples of volcanic and plutonic rocks were collected from the Witkop and Toggekry formations of the Nondweni greenstone belt (App. Table A1). Samples from

Downloaded from http://pubs.geoscienceworld.org/segweb/economicgeology/article-pdf/120/4/903/7306681/5162_netshidzivhe_et_al.pdf
by The Lib. East China Geol Inst. user

the Toggekry Formation are dominated by quartz-sericite schists with minor serpentinites, massive rhyolites, and felsic tuffs. The reddish-brown quartz-sericite schists and quartz-muscovite schists occur as E-W–striking, near vertically dipping individual units reaching up to 15 m in thickness (App. Fig. A2). The felsic metavolcanic rock samples are dominated by quartz, K-feldspar, muscovite, and biotite, with micas defining a strong foliation. These felsic schists represent metamorphosed and strongly deformed rhyolite lavas (Xie et al., 2012; Jele, 2013). The felsic schists are the main host lithology to the Zn-Cu massive sulfide bodies, which are partly exposed in the abandoned Dania and St. James exploration shafts (App. Fig. A2). The nature and origin of this rock association is the primary subject of our paper.

A prominent ridge of black massive homogeneous serpentinite, approximately 170 m in thickness, is located immediately west of the St. James VMS deposit. Toward the northeastern side of the St. James prospect, thick units of steeply dipping massive and homogeneous rhyolite lavas occur at Mount Vernon (App. Fig. A2). The fresh felsic metavolcanic rocks of the Toggekry Formation are black in color. They are conformably overlain by mafic-ultramafic metavolcanic rocks of the Witkop Formation. Versveld (1988) identified a thick basalt to komatiitic basalt lava succession within the Witkop Formation characterized by spinifex textures. The ultramafic lavas reach up to 21 wt % MgO and were originally described as bona fide komatiites (Versfeld, 1988; Wilson et al., 1989; Wilson and Carlson, 1989; Wilson and Versfeld, 1994a). However, the lack of olivine spinifex crystals and the relatively low MgO contents suggest that these metavolcanic rocks are more appropriately referred to as komatiitic basalts (Wilson and Riganti, 2022; this study).

Wilson et al. (1989) conducted a detailed study of outcrops in the Witkop Formation, which they referred to as the "River Section" after the Nondweni River. The same groups of outcrops were sampled in this current study; they are dominated by pyroxene spinifex-textured metabasalts and basaltic lava flows with exceptionally well preserved pillow structures. The pillows are closely spaced with little or no interpillow matrix. In a ~4-m-thick basalt unit overlying komatiitic basalts, the pillow structures reveal a remarkable range in shapes and sizes (0.3–0.6 m across), even within the same stratigraphic unit (App. Fig. A3). The basaltic komatiite unit that underlies the pillow basalt unit exhibits spinifex-like short pyroxene blades in a plagioclase-dominated groundmass (App. Fig. A4). In some River Section outcrops, hyaloclastite and carbonate materials have been observed as interpillow matrix (App. Fig. A3). Rare lava tubes are preserved within the basaltic rock units and are typically filled with quartz and zeolites (App. Fig. A3). The lava tubes vary in size and shape (App. Fig. A3). We also observed ocelli textures within the cores of some pillows (App. Fig. A3). These millimeter- and centimeter-sized ocelli are leucocratic globular features filled with feldspar and carbonate minerals. In general, coalesced ocelli textures in basaltic pillow structures are common in Archean greenstone successions and have also been reported from Isua in West Greenland, Abitibi in eastern Canada, and Barberton and Buffalo River in South Africa (e.g., Viljoen and Viljoen, 1969; Gélinas et al., 1976; Fowler et al., 1987; Wilson and Versfeld, 1994b; Fowler et al., 2002; Sandstå et al., 2011; Netshidzivhe et al., 2023). A ~0.5-m-wide, near-vertical trondhjemite dike intruding the mafic-ultramafic metavolcanic rocks of the Witkop Formation was sampled for U-Pb zircon geochronology to constrain the minimum age of greenstones in the River Section (App. Fig. A3).

Southeast of the River Section, massive lava flows reaching up to 2 m in thickness are characterized by the presence of cumulate zones at the bottom and amphibole-bladed (after pyroxene) to random spinifex zones toward the top (App. Fig. A4). Flow-top breccias commonly show contacts with the cumulate zones of overlying flow units. The breccias are typically <20 cm thick and characterized by a mixture of ~5-cm large rounded and angular fragments of basaltic material (App. Fig. A4). The ~0.4-m-thick lava flow shown in Appendix Figure A4 consists of a slightly altered talc-rich rock that exhibits a fine-crystalline spinifex texture. The lava flow is marked by a sharp internal contact between the basal cumulate zone and the bladed pyroxene spinifex zone. A distinctive succession of spinifex-textured flow units is characterized by the presence of up to 30-cm-long bladed amphibole needles (after pyroxene), which fan out from an individual nucleation point to produce cone structures (App. Fig. A4). Similar cone structures have been reported from pyroxene-bearing komatiite units in the Abitibi greenstone belt of Canada (Arndt and Fleet, 1979).

A range of methods has been applied during this study, and readers are referred to Appendix 1 for descriptions and the reporting of results for reference materials. The range of methods is as follows: optical microscopy; whole-rock major and trace element analyses by X-ray fluorescence (XRF) and inductively coupled plasma-mass spectrometry (ICP-MS); sulfide mineral chemistry by electron probe microanalysis (EPMA); sulfide ore textural characterization by scanning electron microscopy (SEM)-based automated mineralogical analysis; sulfide ore geochemical and C-S analyses by the fire assay and infrared techniques; multiple sulfur isotope analysis by gas-source mass spectrometry; and U/Pb zircon and monazite age determinations by chemical abrasion-isotope dilution-thermal ionization mass spectrometry (CA-ID-TIMS) and laser ablation-multicollector-inductively coupled plasma-mass spectrometry (LA-MC-ICP-MS).

Results

Petrography of the igneous rock samples

The samples from the Paleoarchean Nondweni greenstone belt collected for this study include ultramafic, mafic, and felsic metavolcanic rocks (and a single trondhjemite dike), as well as representative massive sulfide ore samples from the St. James VMS deposit.

The mafic metavolcanic rock samples are dominated by thin blades of spinifex-textured pyroxene, which may be replaced by amphibole. Platy spinifex textures characterize many of the metabasalt and komatiitic basalt samples from the Witkop Formation. Similar to typical olivine spinifex-textured komatiite lava flows, such as those at Pyke Hill in the Abitibi belt in Canada (Pyke et al., 1973), the pyroxene-rich lava flows of the Witkop Formation also preserve basal cumulate zones that grade upward into platy spinifex-textured tops. The main minerals of the platy spinifex zone are long, acicular clinopyroxene and orthopyroxene (up to 2 mm long) set in a

Downloaded from http://pubs.geoscienceworld.org/segweb/economicgeology/article-pdf/120/4/903/7306681/5162_netshidzivhe_et_al.pdf
by The Lib. East China Geol Inst. user

fine chlorite groundmass (App. Fig. A5). The basal zones are dominated by equant actinolite grains and interstitial plagioclase, with subordinate oxide minerals and quartz (App. Fig. A5). The pillowed metabasalts can be texturally divided into a spinifex-textured type and a massive fine-grained type. The relatively coarse spinifex-textured metabasalts are dominated by ~1.8-mm-long euhedral actinolite needles and interstitial plagioclase (App. Fig. A5). Basaltic rocks from the parallel spinifex zone exhibit acicular actinolite in a plagioclase-rich matrix (App. Fig. A5). Randomly oriented thin blades of clinopyroxene are a characteristic feature of the finer grained random spinifex-textured basaltic lava flow tops (App. Fig. A5). Within the Toggekry Formation, very fine grained, massive metarhyolites contain abundant quartz and muscovite, as well as minor alkali feldspar and plagioclase. Chlorite occurs in trace amounts as an alteration phase (App. Fig. A5). Medium-grained quartz-muscovite-biotite schists were sampled in a deep river gully near the St. James Zn-Cu sulfide ore deposit (App. Fig. A5). These felsic schists exhibit a planar fabric resulting in a pronounced foliation. The quartz grains display undulose extinction indicative of high-strain conditions during the shear deformation of the rhyolitic protolith.

The near-vertical inequigranular-textured granitoid dike (NW19-16) that cuts the Paleoarchean greenstones (App. Fig. A5) is composed of medium- to coarse-grained alkali feldspar, plagioclase, and quartz (1–3 mm) set in a finer quartz-biotite-chlorite groundmass. Biotite is the most abundant mafic phase and is mainly found in the groundmass alongside quartz and chlorite. Feldspar is partially saussuritized. The granitoid dike classifies geochemically as a trondhjemite using the Barker (1979) An-Ab-Or diagram (App. Table A1; App. Fig. A6).

Geochemistry of the mafic-ultramafic metavolcanic rocks

The major and trace element concentrations of the 20 mafic and ultramafic volcanic rock samples studied from the Paleoarchean Nondweni greenstone belt are listed in Appendix Table A1. These bulk rock data are recalculated and reported on an anhydrous basis, which is a standard procedure in studies of Archean "greenstones" (Arndt et al., 2008; Barnes and Arndt, 2019; Wilson, 2019). The metavolcanic rocks studied from the Nondweni greenstone belt exhibit variable MgO contents, which is evident from the SiO_2 (41.4–54.8 wt %) versus MgO (4.5–43 wt %) diagram (Fig. 3A). We use the diagram in Figure 3A to show that the mafic-ultramafic rock suite comprises cumulates, komatiitic basalts, and basalts, following the classification scheme of Barnes and Arndt (2019). Using the diagrams by Pearce and Reagan (2019), we show further that the basaltic samples can be subdivided into basalts and basaltic andesites based on their SiO_2 and MgO contents (Fig. 3B). This classification is compatible with the Winchester and Floyd (1977) type diagram, which uses the immobile trace element ratios Zr/Ti and Nb/Y (Fig. 3F). Generally, these metavolcanic rocks show a wide range in TiO_2 (0.1–1.4 wt %). The komatiitic basalts (with <0.5 wt % TiO_2 and >12 wt % MgO) from the Barnes and Arndt (2019) scheme classify as low-silica boninites in the Pearce and Reagan (2019) scheme (Fig. 3B). Their apparent boninitic affinity is also supported by suprachondritic Al_2O_3/TiO_2 (>25) and low Ti/V (<10; Fig. 3C). Boninites are Mg-rich basaltic to andesitic rocks that are relatively rare in Archean terranes (e.g., Smithies et al., 2004). Modern boninites typically form in intraoceanic arcs, forearcs, and back-arc basins (Hickey and Frey, 1982; Crawford et al., 1989), and boninitic compositions are frequently encountered in Phanerozoic ophiolites derived from such convergent margin settings (Stern et al., 2012).

For the basaltic samples, there is a strong variation in TiO_2, with a low-Ti and a high-Ti group (0.8–1.1 vs. 1.3–1.5 wt %; Fig. 3D). In an MgO versus TiO_2 diagram, the basaltic samples fall outside the fields devised by Pearce and Reagan (2019). Using the Ti8 versus Si8 projection, Figure 3E shows that the komatiitic basalts classify as low-silica boninites, whereas four samples from the low-Ti group classify as siliceous high-magnesium basalts. This is due to the high SiO_2 (46.9–53.5 wt %) and MgO (8.2–11.6 wt %) contents of these samples. Using the Zr/Ti versus Nb/Y diagram (Winchester and Floyd, 1977; Pearce, 1996), the mafic-ultramafic metavolcanic rock samples have immobile trace element compositions typical for subalkaline magmatic rocks (Fig. 3F). They follow the tholeiitic trend in a Zr versus Y diagram, where tholeiitic compositions are characterized by Zr/Y between 2 and 4.5 (MacLean and Barrett, 1993; App. Fig. A7).

The primitive mantle-normalized trace element diagrams for the mafic-ultramafic rocks from the Nondweni greenstone belt show a wide variation in their concentrations (App. Fig. A8). The low-Ti basalts exhibit negative Nb, Ta, and Ti anomalies (App. Fig. A8). We note enrichment of the high field strength elements (HFSEs; Zr, Hf, Th, U) and light rare earth elements (LREEs) over the heavy rare earth elements (HREEs; La/Sm_N = 1.7–2.5; Gd/Yb_N = 1.3–1.7). Positive La anomalies are noted for the low-Ti group. The high-Ti group has similar trace element patterns to those of the low-Ti group, but these rocks show a slight enrichment in U-Th and LREEs (La/Sm_N = 1.4–1.7) over the HREEs (Gd/Yb_N ~1.3). A positive Zr-Hf anomaly characterizes the normalized trace element patterns of the high-Ti basalt group (App. Fig. A8).

The komatiitic basalts—which have a boninitic character in terms of their TiO_2, MgO, and SiO_2 compositions—do not exhibit incompatible trace element characteristics of bona fide boninite. Not only are the shapes of the incompatible element patterns different, but the komatiitic basalts also have much lower trace element concentration levels (App. Fig. A8). Apart from the slightly elevated La contents (which may represent a fluid-related overprint), the komatiitic basalts show elevated U concentrations relative to Th and Nb, as well as LREE depletion relative to the HREEs. The komatiitic basalts show a negative Zr-Hf anomaly, which contrasts with the positive anomaly exhibited by several tholeiitic basalt samples (App. Fig. A8). In general, the incompatible trace element concentration levels of the komatiitic basalts are significantly lower than those of modern normal mid-ocean ridge basalts (N-MORBs).

Three serpentinite samples from the Toggekry Formation are designated as cumulate rocks on the basis of their petrography and major element compositions (>40 wt % MgO). These show notable variations in their trace element contents, with U and LREE enrichments (La/Sm_N = 2–2.7) at flat HREE distributions (Gd/Yb_N = 1–1.2; App. Fig. A8).

Geochemistry of the felsic metavolcanic rocks

The major and trace element data for the felsic metavolcanic rocks from the Toggekry Formation in the Nondweni green-

Downloaded from http://pubs.geoscienceworld.org/segweb/economicgeology/article-pdf/120/4/903/7306681/5162_netshidzivhe_et_al.pdf
by The Lib. East China Geol Inst. user

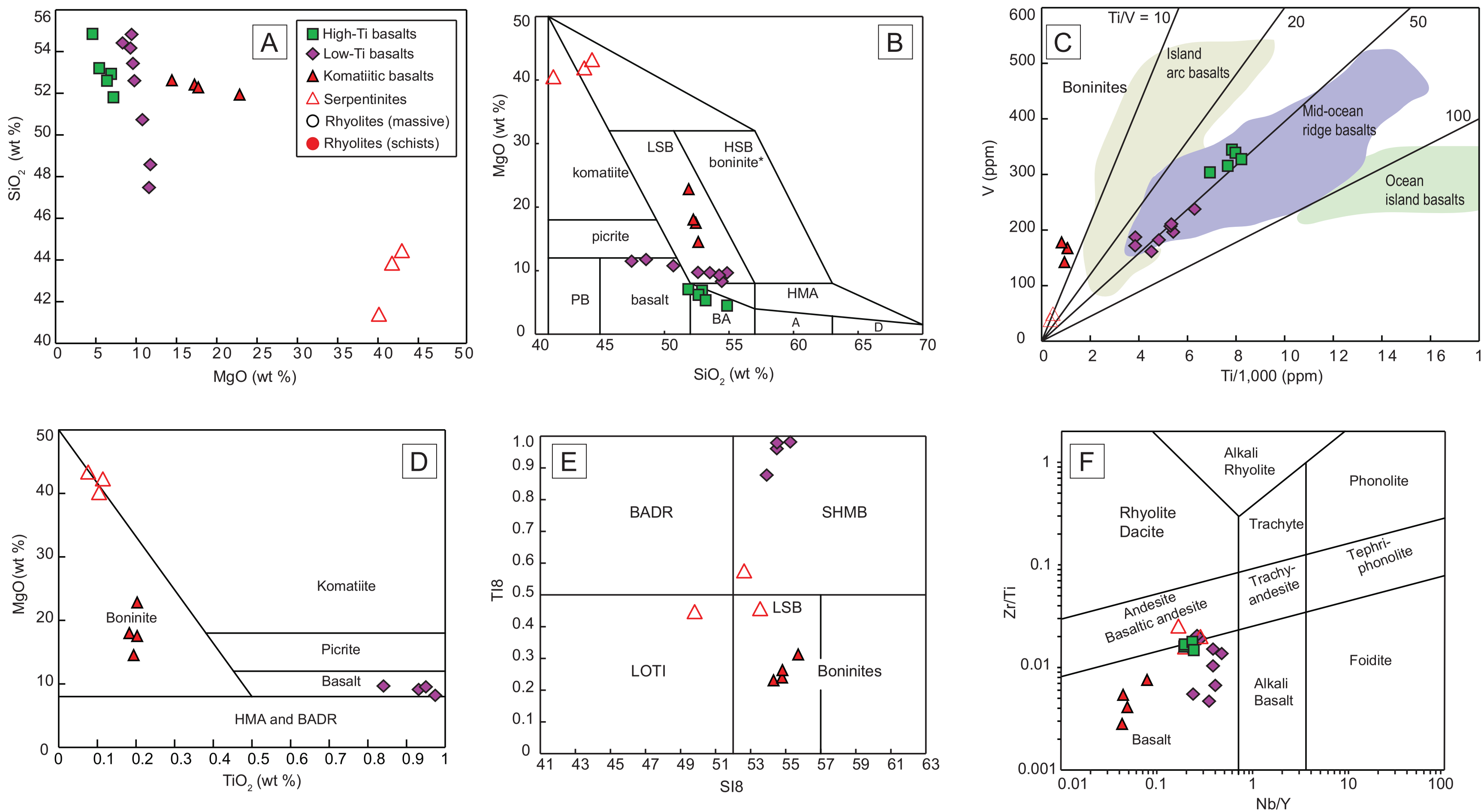

Fig. 3. Geochemistry and classification of the volcanic rocks from the Nondweni greenstone belt. (A) MgO versus SiO_2 diagram showing the chemical variation of the volcanic rocks, where rocks can be classified as basalts, komatiitic basalts, and cumulates. (B) MgO versus SiO_2 classification diagram after Pearce and Reagan (2019). (C) V versus Ti/1,000 used to differentiate boninites from basalts (after Shervais, 1982). (D) TiO_2 versus SiO_2 boninite classification diagram (after Pearce and Reagan, 2019). (E) Ti8 versus Si8 plot used for the classification of boninites. This method of classification is used by obtaining an Si8 value from the MgO-SiO_2 by extrapolating to the line MgO = 8 wt %, where the slope of the bounding lines is utilized and calculated as: $Si_8 = SiO_2 + (MgO - 8)/3.82$ for MgO >8 wt %. The MgO-TiO_2 diagram is used to obtain the Ti_8 value by projecting from the olivine line to MgO = 8 wt % using the equation: $Ti8 = 42TiO/(50 - MgO)$, for MgO >8 wt %. (F) Nb/Y versus Zr/Ti classification diagram, modified after Winchester and Floyd (1977) and Pearce (1996). Abbreviations: A = andesite, BA = basaltic andesite, BADR = basalt-andesite-dacite-rhyolite , D = dacite, HMA = high-Mg andesite, HSB = high-Si boninite, LOTI = low-Ti basalts, LSB = low-silica boninites, PB = picrobasalt, SHMB = siliceous high-magnesium basalts.

Downloaded from http://pubs.geoscienceworld.org/segweb/economicgeology/article-pdf/120/4/903/7306681/5162_netshidzivhe_et_al.pdf
by The Lib. East China Geol Inst. user

stone belt are listed online in Appendix Table A1. Archean felsic metavolcanic rocks can be classified geochemically into FI, FII, and FIII subtypes according to Lesher et al. (1986). This scheme is relevant to our study because it has been used globally as a predictive tool ("prospectivity index") for linking rhyolite geochemistry and VMS fertility in base metal exploration programs. The massive rhyolite samples from the Nondweni greenstone belt classify as FII with $[La/Yb]_N$ = 4–5 and low Zr/Y between 2.9 and 7.5 (App. Fig. A9). The felsic schists classify as FI with $[La/Yb]_N$ = 6–14 and low Zr/Y = 4.5–8.7. These two rhyolite types are recognized as being the most barren with respect to their VMS mineralization potential, whereas the FIII group (not identified at Nondweni) has typically higher prospectivity (Lesher et al., 1986).

The major and trace element compositions of the massive rhyolites and felsic schists are very similar, supporting the idea that the latter represent deformed and sheared rhyolitic lava flows. The massive rhyolites are characterized by high SiO_2 (76.5–82.3 wt %) and K_2O (4.1–6.1 wt %) and low MgO (0.5–1.2 wt %) and TiO_2 (~0.2 wt %) at relatively low loss on ignition (LOI) values between 1.0 and 1.5 wt %. The felsic rhyolitic schists contain 73.2 to 77.9 wt % SiO_2, 2.0 to 3.4 wt % K_2O, 1.5 to 3.8 wt % MgO, and 0.25 to 0.4 wt % TiO_2 at LOI values between 2.8 and 3.0 wt %. The rhyolitic schists display a wide range of Al_2O_3 compositions between 9.5 and 13.3 wt %, which is much wider than the Al_2O_3 range exhibited by the massive rhyolite lava flows (10.1–10.4 wt %).

In primitive mantle-normalized multielement diagrams, the felsic metavolcanic rocks exhibit strong incompatible trace element enrichment, with up to 100 times primitive mantle values. Again, the overlap of certain incompatible trace element contents (U, Th, Nb, Ta, Zr, Hf, Sr) between the massive and schistose rhyolite facies suggests that they share a common origin. This is evident from similar LREE systematics and common negative Ti and Eu anomalies (App. Fig. A10). However, we note that the massive rhyolites have flat HREE patterns (Gd/Yb_N ~1.3) compared to those of the felsic schists, which show HREE depletion relative to the LREEs (App. Fig. A10).

The crosscutting trondhjemite dike is characterized by ~72.2 wt % SiO_2, ~5.96 wt % Na_2O, ~2.26 wt % K_2O, and ~1.1 wt % CaO. The normalized multielement pattern for this sample shows an enrichment in Rb, Cs, and Ba; e.g., ~70 times primitive mantle value for Rb (App. Fig. A6). A negative Nb-Ta and Ti anomaly is observed without Eu and Ba anomalies. We also note a strong LREE enrichment over the HREEs (La/Sm_N = 5.9).

U-Pb zircon and monazite geochronology

The CA-ID-TIMS U/Pb zircon isotope data for rhyolite sample NW19-08/1 from the Toggekry Formation on Mount Vernon are listed in Appendix Table A2, and they are displayed as concordia and weighted mean diagrams in Figure 4A. The five individual zircon analyses yield statistically indistinguishable $^{207}Pb/^{206}Pb$ dates, with a weighted mean age of 3531.91 ± 0.46 Ma (95% confidence interval; mean square of weighted deviates [MSWD] = 0.49). This high-precision U/Pb age is interpreted to mark the timing of felsic volcanism in the lower parts of the Nondweni greenstone belt volcanosedimentary succession. The Th/U ratios of the five single zircon crystals analyzed (0.77–0.78) are characteristic for magmatic zircon in felsic igneous rocks (Hoskin and Ireland, 2000). This first high-precision thermal ionization mass spectrometry (TIMS) U/Pb zircon age, together with the secondary ion mass spectrometry (SIMS) U/Pb zircon age of 3520 ± 6 Ma for a felsic schist sampled some 2 km southeast from our sampling site (Xie et al., 2012), firmly establishes that the Toggekry Formation marks the beginning of the Paleoarchean geologic evolution of the Nondweni greenstone belt.

Felsic schist sample NW19-03/2 from the Toggekry Formation did not yield zircon, but instead we recovered monazite suitable for U-Pb geochronology (App. Table A2). Cathodoluminescence (CL) imaging does not show zoning of these elongated monazite crystals, which have subhedral to prismatic shapes and may contain tiny xenotime inclusions (App. Fig. A11). Fifteen of these metamorphic monazite crystals, ranging between 100 and 150 µm in size, were analyzed by LA-MC-ICP-MS. A total of eight monazite crystals defines a single-age population with an upper intercept discordia age of 3260 ± 14 Ma (Fig. 4B). A similar sample was studied by Jele (2013), who determined a discordia upper intercept age of 3230 ± 5 Ma for 16 metamorphic monazite crystals. These Mesoarchean dates of ca. 3.26 to 3.23 Ga mark a metamorphic overprint of the approximately 3.53-b.y.-old felsic volcanic rocks, probably associated with emplacement of the ca. 3.29 Ga Mvunyana tonalite-trondhjemite-granodiorite batholith now exposed at the flanks of the Nondweni greenstone belt (Matthews et al., 1989; Netshidzivhe et al., 2023).

Zircon was separated from the trondhjemite dike NW19-16, which cuts the mafic-ultramafic metavolcanic rocks of the Witkop Formation. Most zircon crystals are euhedral (prismatic) with some fractures. The crystals analyzed by LA-MC-ICP-MS reach 150 µm in length. Spot analyses on five zircon crystals define an upper intercept $^{207}Pb/^{206}Pb$ age of 3453 ± 52 Ma (Fig. 4C). Importantly, this dike emplacement age provides a minimum age constraint on the greenstone succession of the Witkop Formation, firmly establishing its Paleoarchean origin, succeeding the approximately 3.53-b.y.-old felsic volcanism of the structurally underlying Toggekry Formation.

Major and trace element compositions of the bulk sulfide ore

The bulk sulfide ore major and trace element data are listed in Appendix Table A4, and their variation is controlled mainly by the ore mineralogy and textural associations, including alteration features, the presence of exotic sulfide inclusions, and the nature of the host rocks. The disseminated ore type is characterized by low S concentrations (3–12.2 wt %) at high CaO (~10.2 wt %), MgO (~5.6 wt %), and SiO_2 (49.5 wt %) contents. This is indicative of an association of the disseminated sulfide mineralogy with an abundance of metamorphic silicate minerals as identified in Figures 5 and 6. The massive sulfide ores are more enriched in S (12.2–21.7 wt %) with lower CaO (1.4–1.9 wt %), MgO (0.7–1.9 wt %), and SiO_2 (25–35 wt %) contents.

Mineralogy and textures of the massive and disseminated sulfide ores

Sulfide mineralization is hosted within the felsic schist units of the Toggekry Formation in the Paleoarchean Nondweni

Downloaded from http://pubs.geoscienceworld.org/segweb/economicgeology/article-pdf/120/4/903/7306681/5162_netshidzivhe_et_al.pdf
by The Lib. East China Geol Inst. user

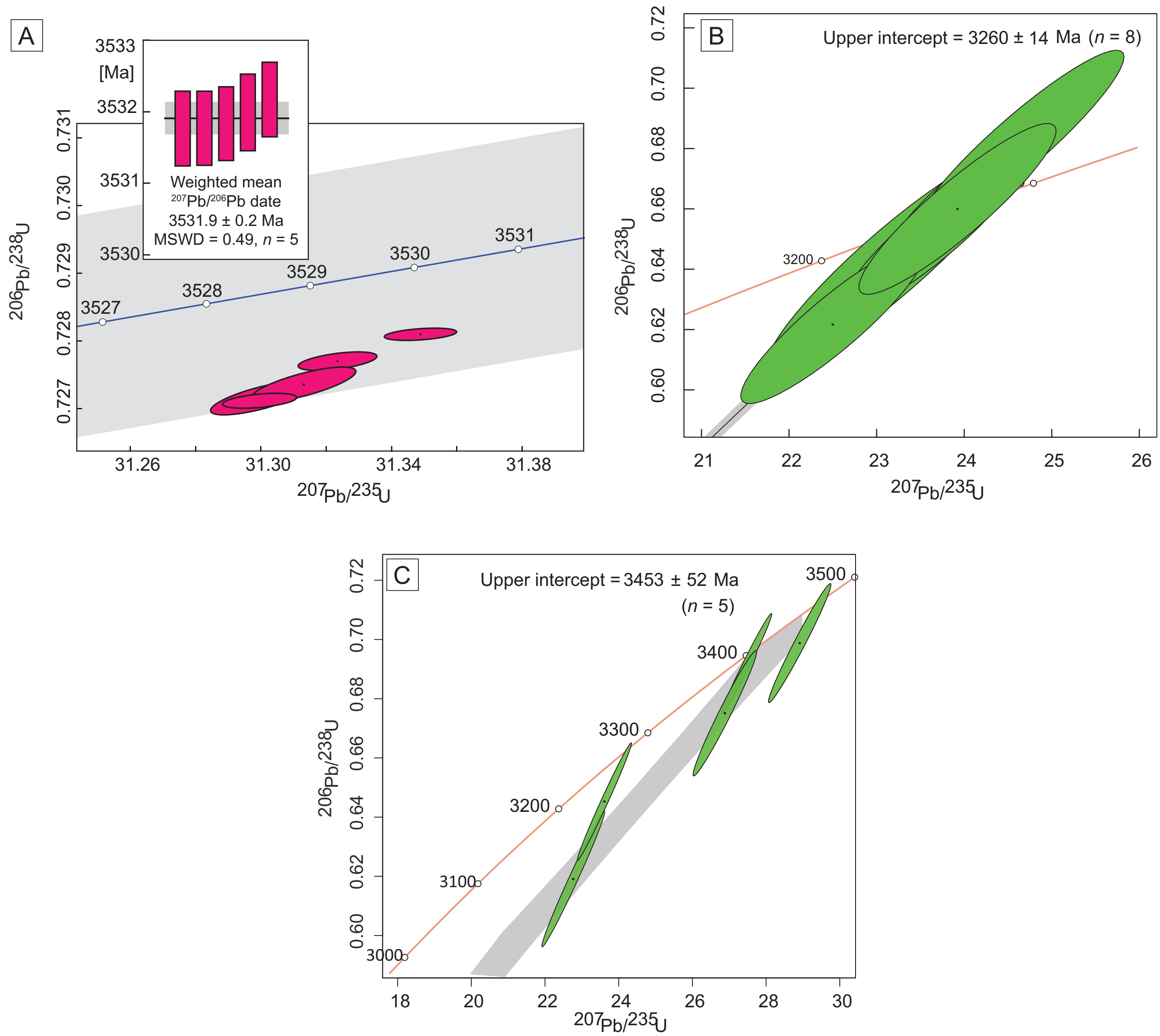

Fig. 4. U-Pb (Wetherill) diagrams for zircon and monazite. (A) Weighted mean and concordia diagrams for rhyolite (massive) from the Toggekry Formation. (B) Weighted mean and discordia diagrams for rhyolite schist from the northern outcrop of Toggekry Formation. (C) Discordia diagram from a trondhjemite dike of the Witkop Formation. Age calculations and data displayed conducted using IsoplotR (Vermeesch, 2018). MSWD = mean square of weighted deviates.

greenstone belt (Fig. 2). Our study shows that the relatively small orebodies are characterized by both massive sulfides and disseminated sulfides, which constitute an overall similar mineralogy. However, the massive sulfide ore is more voluminous and dominated by sphalerite ([Zn,Fe]S; ~35%), chalcopyrite ($CuFeS_2$; ~30%), pyrrhotite (FeS; ~20%), and pyrite (FeS_2; ~10%), with minor to trace amounts of galena (PbS; <5%) and acanthite (Ag_2S; <<1%; i.e., trace component). Sphalerite occurs as 2- to 3-mm large recrystallized grains that may contain small chalcopyrite inclusions (Fig. 5A). The sphalerite grains contain on average 57.8 wt % Zn and 33.6 wt % S, with significant Fe contents (7.9 wt % Fe on average; App. Table A3). Chalcopyrite contains on average 34.2 wt % Cu, 30.2 wt % Fe, and 34.8 wt % S. Pyrrhotite contains on average 59 wt % Fe and 39 wt % S. It typically forms recrystallized reaction rims when in contact with Fe-rich sphalerite (Fig. 5B). This texture is only observed in the massive sulfide ore samples (App. Fig. A12) and is probably related to alteration or metamorphism. Pyrrhotite also occurs as large recrystallized grains with annealing textures forming high-angled triple-point junctions with sphalerite grains. In samples where chalcopyrite does not occur as inclusions or blebs in sphalerite, these two sulfide phases form an anhedral texture with shared grain boundaries (Fig. 5C). In these samples, sphalerite and chalcopyrite are present in approximately equal proportions (NW19-02/1A). Small galena grains are commonly intergrown with large chalcopyrite grains but also with small chalcopyrite inclusions (Fig. 5D). The silver sulfide acanthite is typically found as rare single grains, which range between 10 and 40 μm in diameter and are associated with chalcopyrite and clinozoisite (Fig. 5E).

Downloaded from http://pubs.geoscienceworld.org/segweb/economicgeology/article-pdf/120/4/903/7306681/5162_netshidzivhe_et_al.pdf
by The Lib, East China Geol Inst. user

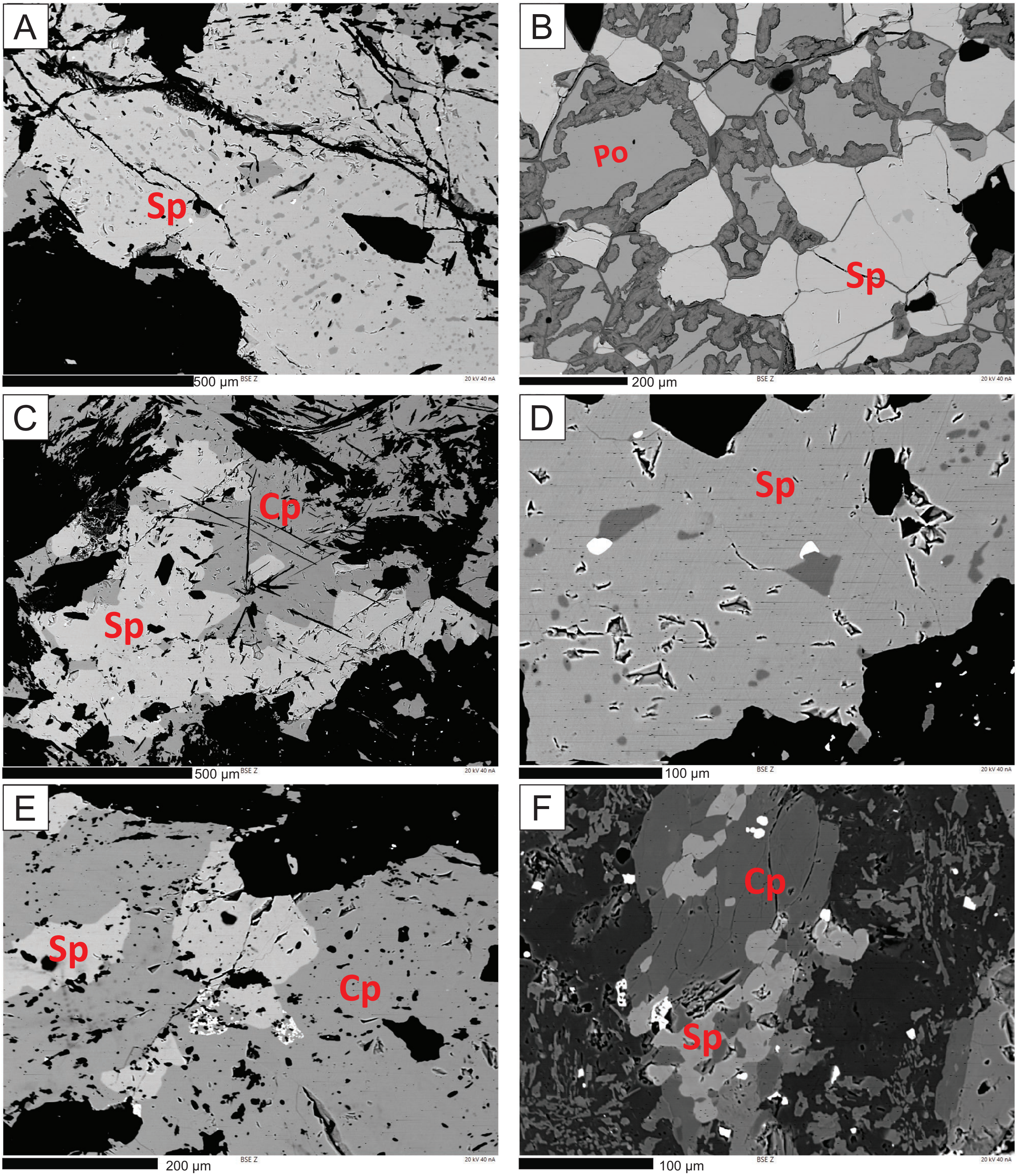

Fig. 5. Backscattered electron (BSE) images of the massive and disseminated ores of the Nondweni greenstone belt. (A) Large, recrystallized sphalerite with chalcopyrite inclusions. (B) Pyrrhotite alteration around grain boundaries forming triple point junctions with sphalerite. (C) Sphalerite and chalcopyrite forming a xenomorphic texture surrounded by gangue silicate minerals. (D) Large sphalerite with chalcopyrite inclusions intergrown with galena. (E) Chalcopyrite and sphalerite with bright aggregates of acanthite intergrown with chalcopyrite. (F) Chalcopyrite intergrown with sphalerite and galena from the disseminated ore type. Abbreviations: Cp = chalcopyrite, Po = pyrrhotite, Sp = sphalerite.

Downloaded from http://pubs.geoscienceworld.org/segweb/economicgeology/article-pdf/120/4/903/7306681/5162_netshidzivhe_et_al.pdf
by The Lib. East China Geol Inst. user

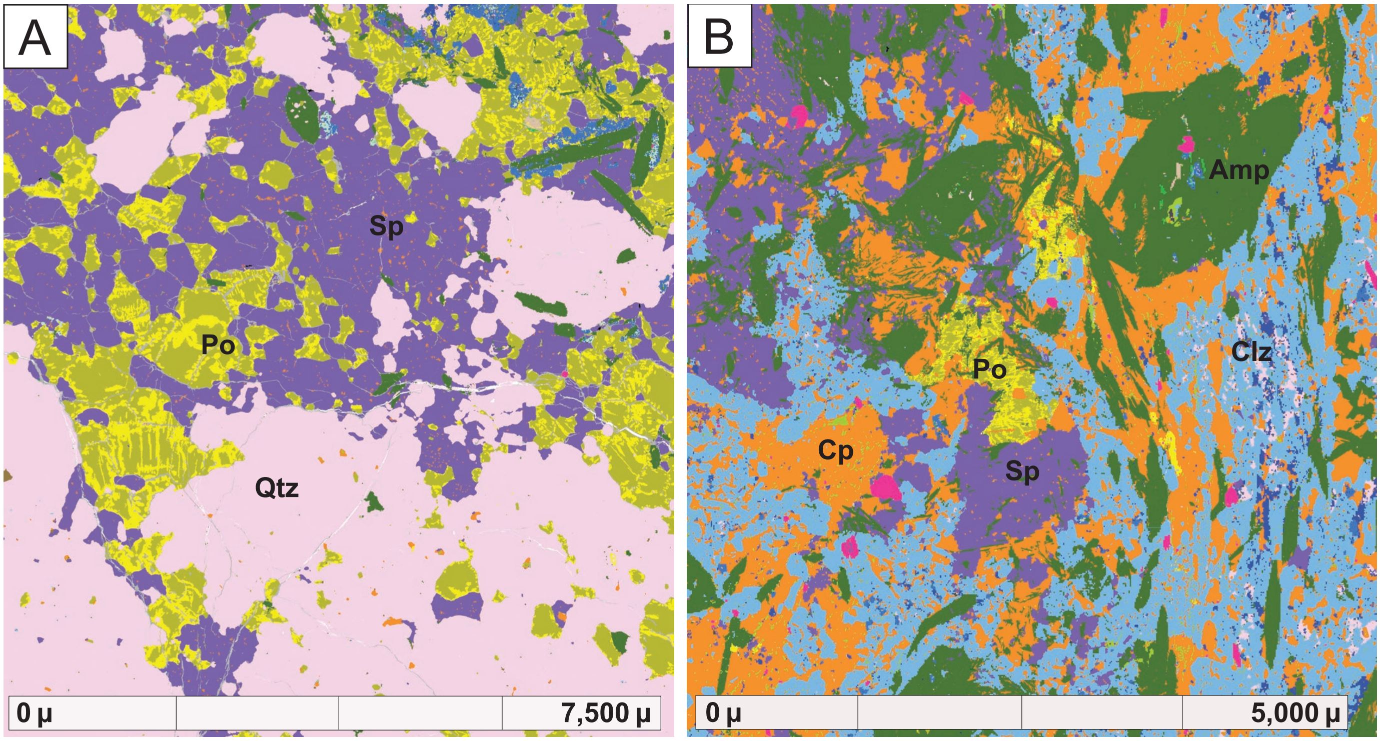

Fig. 6. GXMAP mineral maps showing the distribution of the sulfides and associated gangue minerals. (A) Massive sulfide ore sample NW19-2/1B dominated by pyrrhotite and sphalerite (with fine-grained inclusions of chalcopyrite). Gangue minerals include quartz, amphibole, and feldspar. (B) Sample NW19-2/1A dominated by chalcopyrite, sphalerite, and pyrrhotite (with pyrite along grain boundaries) as the main sulfide minerals with amphibole, apatite (pink), clinozoisite, and trace K-feldspar and quartz. Abbreviations: Amp = amphibole, Clz = clinozoisite, Cp = Chalcopyrite, Po = pyrrhotite, Qtz = quartz, Sp = sphalerite.

Disseminated sulfide ores (NW19-02/7) are less abundant and typically dominated by chalcopyrite, with traces of pyrite and pyrrhotite. Sphalerite is also present in trace amounts, typically intergrown with chalcopyrite (Fig. 5F). A distinctive feature of the disseminated sulfide ores is the development of mineralogical banding with an alignment of the sulfides parallel to the main foliation plane of the rock unit (App. Fig. A12). The gangue mineral assemblage consists of low-grade greenschist facies metamorphic phases including clinozoisite, prehnite, and pumpellyite, plus abundant quartz (Fig. 6). The major and minor element compositions of the main minerals identified are fairly homogeneous across the sample suite (App. Table A3).

The massive sulfide ores have high Zn (5.3–25.9 wt %), Cu (1.4–5.8 wt %), and Pb (0.17–0.41 wt %) contents indicative of the abundance of sphalerite, chalcopyrite, and galena, respectively. In contrast, the disseminated sulfide ore samples are highly diluted by silicate minerals and generally contain <1 wt % Cu, ~7 wt % Fe, <0.2 wt % Pb, and only ~0.08 wt % Zn. The compositional differences and variations among the two ore types are displayed in Appendix Figure A13. The disseminated sulfide ore sample NW19-02/7, with the lowest sphalerite content, has the lowest Zn/Cu ratio of ~0.09. Sample NW19-02/2B, with elevated Zn content (25.9 wt % Zn), shows the highest Zn/Cu ratio of ~104 and Fe/Cu ratio of ~23 (App. Fig. A13), indicative of modal sphalerite. The trace element compositions of the massive and disseminated sulfide ore type are also distinctively different. The massive sulfide ore samples are characterized by an enrichment in Pb (~4,000 ppm), Ag (>100 ppm), Co (33–117 ppm), and Cd (up to 573 ppm), which is due to the association of modal acanthite and galena. In contrast, the Ag concentrations of the disseminated sulfide ore samples are below method detection limit (<0.5 ppm), with very low concentration levels of Pb (~168 ppm), Co (~11 ppm), and Cd (~3.5 ppm).

Sulfur isotope compositions of the bulk sulfide ores and selected metavolcanic rocks

We measured the bulk $\delta^{33}S$, $\delta^{34}S$, and $\delta^{36}S$ compositions of five base metal sulfide ore samples (massive and disseminated types), as well as two massive rhyolite samples from the Toggekry Formation and three basalt samples from the Witkop Formation (App. Table A5; Fig. 7). The $\delta^{34}S$ values for the sulfide ore samples are relatively low, between –2.6 and –1.4‰, with corresponding $\Delta^{33}S$ values between –0.54 and –0.53‰. The $\Delta^{36}S$ values of these samples vary between –0.14 and +0.57‰. In general, the $\delta^{34}S$ compositions of the sulfide ores from the Nondweni greenstone belt are similar to those reported from other Archean VMS deposits worldwide (–2 to +2‰ $\delta^{34}S$; Franklin et al., 1981; Schwarz-Schampera et al., 2010; Sharman et al., 2015), albeit at the light isotopic end of the known $\delta^{34}S$ range (Fig. 7).

The three basalt samples from the Witkop Formation are characterized by positive $\delta^{34}S$ values between 0.6 and 1‰, with corresponding near-zero $\Delta^{33}S$ values (–0.05 to –0.03‰) and $\Delta^{36}S$ compositions ranging between –0.4 and +0.19‰. The

Downloaded from http://pubs.geoscienceworld.org/segweb/economicgeology/article-pdf/120/4/903/7306681/5162_netshidzivhe_et_al.pdf
by The Lib. East China Geol Inst. user

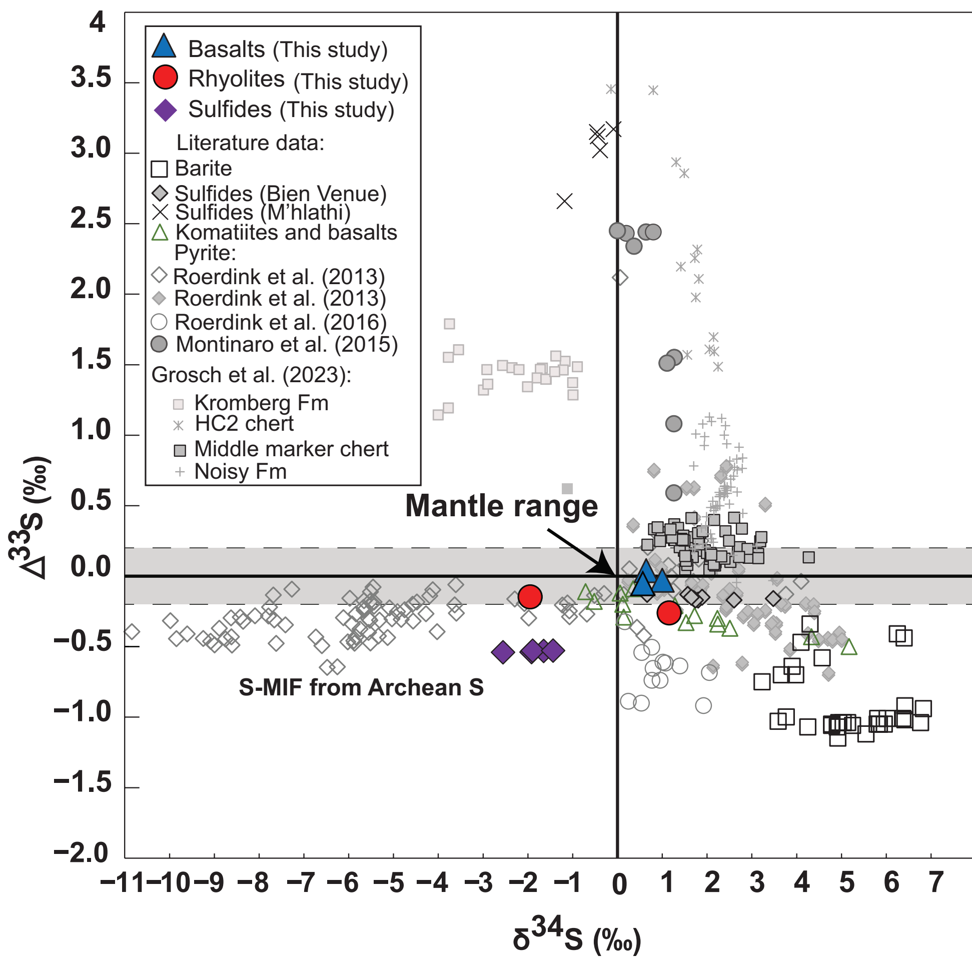

Fig. 7. Multiple sulfur isotopic compositions of the Nondweni greenstone belt showing $\delta^{34}S$ and $\Delta^{33}S$ values for the massive sulfide ores and the surrounding rhyolites and basalts. Error bars are smaller than point size and are not discernible on the plot. The mantle S isotope composition is shown with a solid black line (Labidi et al., 2013), and the shaded gray field represents the traditional mass-dependent fractionation field of Farquhar and Wing (2003). Sulfur isotope compositions shown for comparison are from Paleoarchean rocks, sulfide, and barite in the Barberton greenstone belt (Bao et al., 2007; Roerdink et al, 2012, 2013, 2016; Montinaro et al., 2015; Grosch et al., 2023). S-MIF = sulfur mass-independent fractionation.

two rhyolite samples from the Toggekry Formation have similar $\Delta^{33}S$ compositions of –0.3 and –0.2‰, and comparable $\Delta^{36}S$ compositions of +0.3 and +1.2‰, but they have markedly different $\Delta^{34}S$ values. Rhyolite sample NW19-08/2 has a $\Delta^{34}S$ of +1.2‰, similar to the isotopic signature of the basalts, whereas rhyolite sample NW19-08/3 has a much lower $\Delta^{34}S$ composition of –1.9‰, overlapping with the sulfide ores (Fig. 7).

Discussion

Constraints on the age of the St. James deposit: World's oldest VMS-type mineralization?

Determining the ages of ancient VMS deposits by direct geochronological methods applied to the sulfide minerals is notoriously difficult (Stein, 2014; Stein and Hannah, 2015). Poor precision due to the low Os contents of hydrothermal sulfides has been a major source of limitation for using the Re-Os method for dating VMS deposits. The lack of suitable reference materials further compromises the quality of sulfide mineral geochronology. Nevertheless, the Re-Os method has gained acceptance during the last decade and is now widely employed in magmatic and hydrothermal sulfide ore deposit studies. Alternatively, high-precision U/Pb geochronology of the host volcanic rock units can provide valuable insights into the age of the sulfide mineralization, assuming that magmatism and sea-floor hydrothermal activity were coeval.

Our study confirms previous suggestions (e.g., Hofmann et al., 2019) that the felsic metavolcanic rocks of the Toggekry Formation are the immediate host of the relatively small VMS-type mineralization at the St. James site (Fig. 2). A felsic schist sample yielded a SIMS U/Pb zircon age of 3520 ± 6 Ma (Xie et al., 2012), and our massive rhyolite sample NW19-08/1 yielded a TIMS U/Pb zircon age of 3531.91 ± 0.46 Ma (Fig. 4A; App. Table A2). These high-precision dates are best interpreted as emplacement ages of the rhyolitic lavas from the Toggekry Formation at ca. 3.53 to 3.52 Ga and, by inference, this Paleoarchean age approximates the timing of VMS-type mineralization within the felsic volcanic rock units. Tight folding and shearing at relatively low metamorphic conditions affected certain parts of the Nondweni greenstone belt during the latest Paleoarchean to early Mesoarchean at ca. 3.25 to 3.23 Ga, as evident from the U/Pb monazite ages ob-

Downloaded from http://pubs.geoscienceworld.org/segweb/economicgeology/article-pdf/120/4/903/7306681/5162_netshidzivhe_et_al.pdf
by The Lib, East China Geol Inst. user

tained for felsic schist samples in our study and also by Jele (2013). The Mesoarchean was also a time of regional tonalite-trondhjemite-granodiorite magmatism and associated metamorphism in and around the Nondweni greenstone belt. This includes the Mvunyana batholith exposed along the eastern and southern flanks, which yielded a whole-rock Rb-Sr age of 3290 ± 33 Ma (Matthew et al., 1989) and U/Pb zircon ages between 3286 and 3260 Ma (Netshidzivhe et al., 2023). Given that the VMS-type mineralization hosted by the 3.53- to 3.52-b.y.-old felsic schists also shows signs of ductile to brittle deformation and contains a low-grade metamorphic silicate mineral assemblage (Fig. 6), it is reasonable to argue that the sulfide ores formed before 3.25 Ga. Moreover, given that the felsic volcanic rocks of the Toggekry Formation are overlain by mafic-ultramafic volcanic rocks of the Witkop Formation, which is cut by approximately 3.45-b.y.-old granitoid dikes (Fig. 4C), it is highly probable that the St. James VMS deposit has a Paleoarchean age, probably similar to that of the felsic volcanism at ca. 3.53 Ga.

Global data sets suggest that >50% of the recorded VMS deposits are hosted by felsic volcanic rocks in addition to basalts and related rocks (Franklin et al., 1981, 2005; Lentz, 1998; Piercey, 2010; Hannington, 2014). The geologic record of the ca. 3.53 Ga Toggekry Formation appears to be unique because, to the best of our knowledge, no other Paleoarchean greenstone belts are recognized to host VMS-type mineralization at this early stage in Earth history. For example, the St. James VMS deposit predates the ca. 3.47 Ga felsic-hosted VMS mineralization in the Duffer Formation of the Pilbara craton in Australia, which was considered to be the oldest of its kind (Hickman, 2023). Felsic-hosted VMS deposits only became more abundant during the Neoarchean, with numerous examples from the Yilgarn craton in Australia (Hollis et al., 2015) and the Superior craton in Canada (Lesher et al., 1986). Given the antiquity of the ca. 3.53 Ga St. James VMS deposit in the Nondweni greenstone belt of the Kaapvaal craton in South Africa, there is an opportunity to probe the ore-forming processes that took place on and directly beneath the Paleoarchean sea floor.

Possible origins of the ca. 3.53 Ga rhyolites and associated VMS-type mineralization

It is recognized that volcanic host rock compositions can influence levels of base metal enrichment within VMS-type ore deposits (Lesher et al., 1986; Fouquet et al., 2010). For example, hydrothermal sulfide deposits hosted within ultramafic rocks are typically dominated by Cu, whereas those hosted by felsic volcanic rocks are typically enriched in Zn, Pb, Ag, As, Sb, and Au (Franklin et al., 1981; Barrie and Hannington, 1999; Binns and Scott, 1993; Candela, 2003). This relationship appears to also exist for the Zn-Pb-Ag–rich VMS-type mineralization at the St. James site hosted by the ca. 3.53 Ga felsic schists of the Toggekry Formation. In general, rhyolites and their deformed schistose equivalents are a volumetrically minor but ubiquitous volcanic component of mafic-ultramafic–dominated Archean supracrustal belts (e.g., Laurent et al., 2020), as is the case in the Nondweni greenstone belt on the Kaapvaal craton. Time-equivalent felsic volcanism occurred in the Barberton greenstone belt farther north on the Kaapvaal craton as recorded by the ca. 3.53 Ga Theespruit Formation (Viljoen and Viljoen, 1969; Kröner et al., 1996). In the following sections, we aim to further explore the origins and possible petrogenetic links between the felsic volcanism and VMS-type mineralization within the ca. 3.53 Ga Toggekry Formation of the Nondweni greenstone belt. This hydrothermal Zn-Cu-Pb-Ag sulfide mineralization is among the oldest of its kind globally and thus sheds light into early Earth processes (cf. Cawood and Hawkesworth, 2015).

For the archetypal Barberton greenstone belt, the identification of Paleoarchean felsic volcanism resulted in the development of geodynamic models invoking an intraoceanic arc environment, where melting was induced by "hot" subduction zone processes (e.g., de Ronde and de Wit, 1994; Lowe, 1994; de Wit, 2004; Furnes et al., 2013). Two petrogenetic models have been proposed to explain the origins of rhyolites in close spatiotemporal association with mafic-ultramafic volcanic rock suites in Archean greenstone belts: (1) extreme fractional crystallization of basaltic magmas (similar to rhyolites on Iceland; Carmichael, 1964; Macdonald et al., 1990; Furman et al., 1992), with minor assimilation of altered wall rocks (Sigurdsson and Sparks, 1981; Macdonald et al., 1987; McGarvie et al., 1990; Nicholson et al., 1991); and (2) partial melting of hydrated mafic-ultramafic crust that had undergone sea-floor hydrothermal alteration (e.g., Óskarsson et al., 1982, 1985; Condomines et al., 1983; Thy et al., 1990; Sigmarsson et al., 1991, 1992; Jónasson, 1994).

Using PETROMODELER, a Microsoft Excel spreadsheet developed by Ersoy (2013), we tested whether the ca. 3.53 Ga rhyolites of the Toggekry Formation could be linked to the tholeiitic basalts of the Nondweni greenstone belt via partial melting at shallow crustal depths (<5 km), probably aided by previous intensive sea-floor hydrothermal alteration to lower the melting point (Spulber and Rutherford, 1983; Zierenberg et al., 2013). For such a batch melting model, we used basalt sample NW19-12 (App. Table A1 lists the trace element data) as the starting composition. Relevant mineral/melt REE partition coefficients were taken from the GERM database (https://earthref.org/GERM; App. Table A6). The model output results are normalized to the chondrite REE values of McDonough and Sun (1995) and displayed in Figure 8. The modeled rhyolites have near identical REE compositions compared to our rhyolite samples in cases where the tholeiitic basalt source was melted between 12 and 17%. At lower degrees of partial melting (5–10%), the rhyolite model melts have similar HREE contents and distributions to the rhyolites from the Toggekry Formation; however, their LREE concentrations are too high (Fig. 8A). This simple, trace element-forward model, together with constraints from experimental petrology (Spulber and Rutherford, 1983; Zierenberg et al., 2013), suggests that moderate degrees of partial melting of hydrated basaltic crust can give rise to confined volumes of rhyolitic magmas similar to those found in the Paleoarchean Nondweni greenstone belt. The most favorable setting for this process to occur was probably an oceanic spreading ridge system in a back-arc environment, where the mafic-ultramafic ocean floor had been intensively hydrothermally altered and kept at elevated temperatures over prolonged periods of time so that it could locally melt at low pressures (<2 kbar; Spulber and Rutherford, 1983; Zierenberg et al., 2013) and produce batches of rhyolitic magma near the surface. Such an envi-

Downloaded from http://pubs.geoscienceworld.org/segweb/economicgeology/article-pdf/120/4/903/7306681/5162_netshidzivhe_et_al.pdf
by The Lib. East China Geol Inst. user

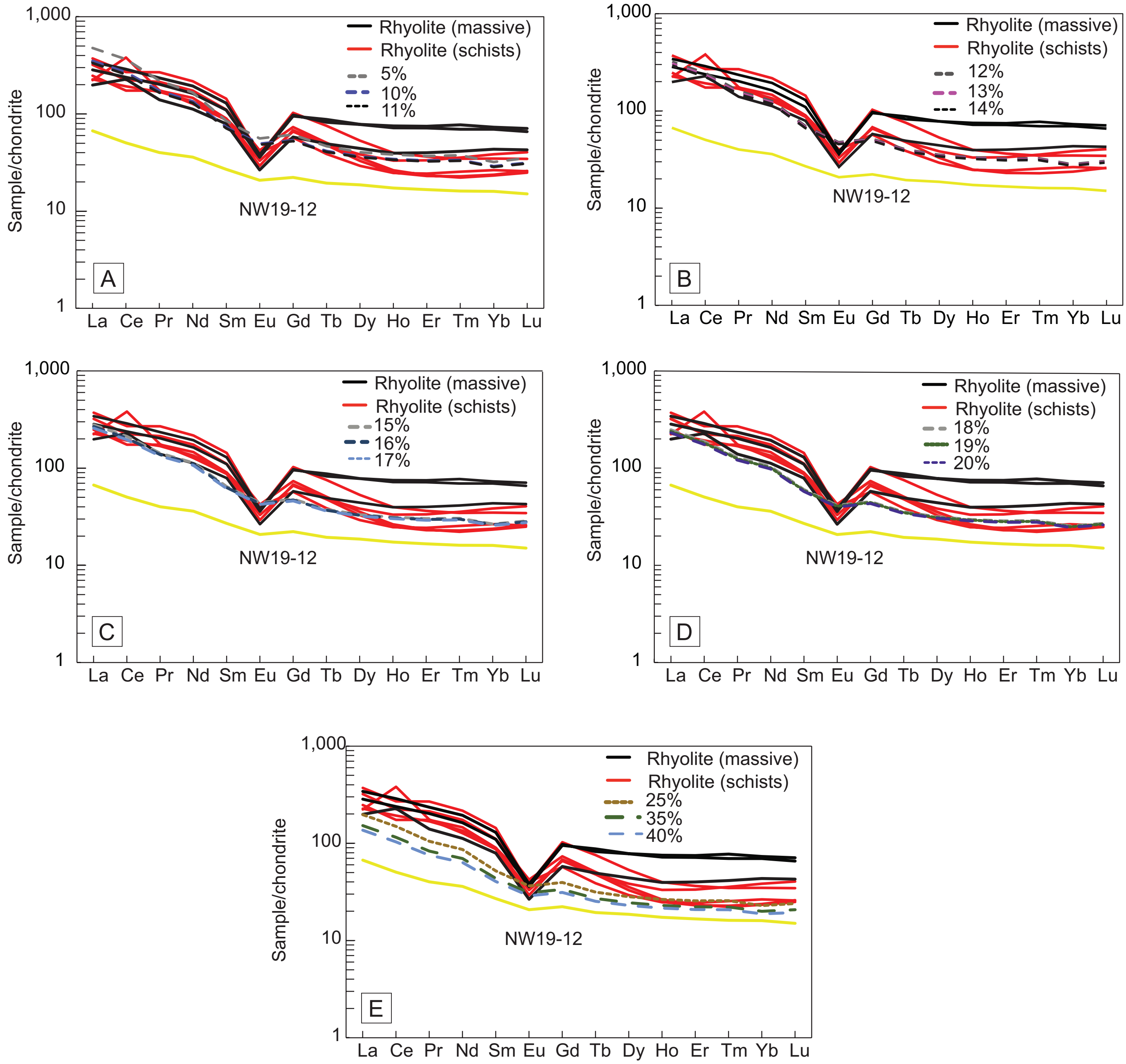

Fig. 8. Chondrite-normalized rare earth element (REE) plots showing the geochemical modeling of the Nondweni volcanic lavas. Comparisons are made for various degrees of partial melting of a basalt (sample NW19-12) from the Witkop Formation. Normalizing values from McDonough and Sun (1995).

ronment is also known to generate hydrothermal VMS-type deposits linked directly to the ocean floor heat anomalies that may give rise to local submarine felsic volcanism (Hannington, 2014). Our preferred model of VMS deposit formation in a back-arc rift environment at ca. 3.53 Ga assumes the operation of subduction zone processes. For the Kaapvaal craton, nitrogen isotope evidence from Archean placer diamonds suggests that crustal materials had been transferred to >150-km depth before 3.5 Ga, which is only possible by modern-style plate tectonics involving subduction (Smart et al., 2016).

Implications of the S-MIF signature in the VMS-type mineralization at St. James

For VMS deposits, the sources of sulfur and the origins of ore-forming fluids can be constrained by investigating their multiple sulfur isotope compositions. Multiple sulfur isotopes serve as a crucial tool in tracing the Archean sulfur cycle preserved in the rock record (Farquhar et al., 2000, 2002; Farquhar and Wing, 2003; Johnston, 2011). This is because they allow for the identification of various sulfur sources, which can be distinguished on the basis of diagnostic sulfur isotope signatures. Mass-independent fractionation of sulfur isotopes

Downloaded from http://pubs.geoscienceworld.org/segweb/economicgeology/article-pdf/120/4/903/7306681/5162_netshidzivhe_et_al.pdf
by The Lib. East China Geol Inst. user

(S-MIF) has been recorded globally in many rock and mineral samples older than 2.45 Ga but is essentially absent in sedimentary rock samples younger than 2 Ga (Farquhar et al., 2000; Farquhar and Wing, 2003). According to Farquhar et al. (2000), S-MIF signatures were produced in Earth's oxygen-free/poor atmosphere that dominated before 2.45 Ga, where SO_2 from volcanic activity underwent photolysis reactions. This mechanism resulted in reduced sulfur species with positive $\Delta^{33}S$ values and complementary oxidized sulfur species with negative $\Delta^{33}S$ values deviating from normal sulfur mass-dependent fractionation (MDF) marked by $\Delta^{33}S = 0‰$ (Farquhar et al., 2000). Originally, S-MIF signatures were defined by Farquhar and Wing (2003) as $\Delta^{33}S = 0 \pm 0.2‰$, but more recently the threshold value was extended by LaFlamme et al. (2018) to account for MDF processes that can generate $\Delta^{33}S = 0 \pm 0.5‰$.

Results from previous multiple sulfur isotope work on Paleoarchean rocks, sulfide minerals, and barite from the nearby well-studied Barberton greenstone belt are used here for comparison (see Bao et al., 2007; Roerdink et al., 2012, 2013, 2016; Montinaro et al., 2015; Grosch et al., 2023). Our study reveals that the basalts, rhyolites, and sulfide ore samples from the St. James VMS deposit have distinct $\Delta^{33}S$ values across a range of $\delta^{34}S$ compositions (Fig. 7). The basaltic samples have unfractionated mantle-like sulfur isotope compositions, revealed by both their $\delta^{34}S$ (+0.6 to +1‰) and $\Delta^{33}S$ (–0.05 to –0.03‰) values, which are in good agreement with a magmatic sulfur source exhibiting near-zero multiple sulfur isotope values (e.g., Farquhar et al., 2002; Labidi et al., 2012, 2013, 2014). It is clear from Figure 7 that the basaltic samples' sulfur isotope compositions do not overlap with those reported for mantle-derived komatiites and tholeiitic basalts ($\delta^{34}S$ = –0.7 to +5.2‰ and $\Delta^{33}S$ = –0.5 to –0.09‰) from the Barberton greenstone belt (Montinaro et al., 2015). Such a wide range of sulfur isotope compositions falls outside the established range of mantle values. Mantle-derived silicate melts are known to be sulfur deficient after ascent to crustal levels, and any S-MIF signatures that primitive magmatic rocks record must have originated from other geochemical reservoirs closer to Earth's surface. The observed difference in the sulfur isotope compositions between primitive volcanic rocks from the two Paleoarchean greenstone belts on the Kaapvaal craton suggests that the Nondweni tholeiites record a true mantle sulfur isotope signature without a history of atmospheric sulfur interaction, as is suggested only for the Barberton volcanic rock data.

The sulfur isotope compositional range observed for the two rhyolite samples reveals slightly fractionated $\Delta^{33}S$ values (–0.26 and –0.15‰ at $\delta^{34}S$ values of –1.9 and +1.2‰), with $\Delta^{36}S$ values of +0.31 and +1.19‰ (Fig. 7). These nonzero $\Delta^{33}S$ compositions of the rhyolites are not considered to present a significant S-MIF signature. The $\delta^{34}S$ values of these rhyolite samples may record the partial melting process of seawater-altered basaltic oceanic crust, because altered modern oceanic basalts have $\delta^{34}S$ values between –6 and +0.9‰ (Alt and Shanks, 2011; Evans et al., 2014). Fragments of Archean oceanic crust, as represented by cratonic eclogite xenoliths in kimberlites, have $\delta^{34}S$ values between –13 and +20‰ (e.g., Evans et al., 2014; Walters et al., 2019; Burness et al., 2021). The small nonzero $\Delta^{33}S$ deviation recorded by the Nondweni rhyolites may reflect a small contribution from sedimentary material as part of the altered oceanic crustal unit that underwent local melting to produce small batches of felsic magma (Fig. 8). An alternative interpretation of the slightly negative $\Delta^{33}S$ and low $\delta^{34}S$ values measured for the rhyolites could be a minimal contribution of seawater sulfate that was incorporated into the felsic volcanic rocks during alteration. A possible role of Archean seawater sulfate is explained by the presence of Paleoarchean barite, which carries negative $\Delta^{33}S$ and positive $\delta^{34}S$ signatures at sites in the Barberton greenstone belt (Roerdink et al., 2013; Grosch et al., 2023). Such signatures, indicative of sea-floor alteration, may indeed be recorded by the rhyolites from the Nondweni greenstone belt (Fig. 7). Incorporation of seawater sulfur into volcanic rocks via thermochemical or biological sulfate reduction has been suggested for Paleoarchean sea-floor altered basalts from the Pilbara craton in Australia (Aoyama and Ueno, 2018).

In contrast to the rhyolites and basalts, the VMS-type mineralization at St. James in the Nondweni greenstone belt has a more clearly resolved S-MIF signature of $\Delta^{33}S$ = –0.53‰ at consistently negative $\delta^{34}S$ values that fall mostly within the range of Archean VMS deposits from localities worldwide ($\delta^{34}S$ = –2 to +2‰; Franklin et al., 1981; Sharman et al., 2015; Huston et al., 2023). Negative $\delta^{34}S$ attests to low sulfate concentrations that appear to be typical for Archean seawater (Farquhar et al., 2010; Huston et al., 2023). Furthermore, we show that the St. James sulfide ore sulfur isotope compositions are different from those of the approximately 3.25-b.y.-old Bien Venue and M'hlati VMS-type deposits in the Barberton greenstone belt (Fig. 7). The isotope compositions of the Bien Venue sulfide ores are characterized by positive $\delta^{34}S$ values ranging between +0.7 and +3.5‰, with corresponding nonzero negative $\Delta^{33}S$ values between –0.17 and –0.12‰ (Montinaro et al., 2015). Such compositions do not indicate the presence of an S-MIF signature for the Bien Venue ores and were interpreted as a vestige of an unfractionated, purely magmatic sulfur source for this Mesoarchean VMS-type mineralization (Montinaro et al., 2015). In contrast, the M'hlati sulfides exhibit highly positive $\Delta^{33}S$ values (+2.66 and +3.17‰) at negative $\delta^{34}S$ compositions (–1.2 and –0.1‰). The strongly positive S-MIF signature was suggested to be due to photolytic elemental sulfur incorporation from the atmosphere into submarine sulfide precipitation (Montinaro et al., 2015). Furthermore, the sulfur isotope compositions of Archean sedimentary pyrite and barite gave rise to various hypotheses regarding the isotopic records of Archean surface environments in the Barberton greenstone belt. A study on sediment-hosted sulfides was conducted by Roerdink et al. (2013) exploring the ca. 3.2 Ga Barite Valley deposit within the Fig Tree Group. Their data identified the widespread presence of pyrite with distinctive negative $\delta^{34}S$ and $\Delta^{33}S$ signatures (Fig. 7). They interpreted these results as being inconsistent with purely atmospheric processes and instead proposed microbial reduction of seawater sulfate as the main contributing factor. In a subsequent study by Roerdink et al. (2016), pyrite was analyzed from the ca. 3.52 Ga Londozi barite of the Theespruit Formation in the Barberton greenstone belt. The authors identified S-MIF signatures and argued that they record photochemical processes within a pre-3.5 Ga atmosphere, from which sulfur found its way into

Downloaded from http://pubs.geoscienceworld.org/segweb/economicgeology/article-pdf/120/4/903/7306681/5162_netshidzivhe_et_al.pdf
by The Lib. East China Geol Inst. user

hydrothermal systems. The proposed model suggested mixing of 10% recycled photolytic and 90% juvenile magmatic sulfur (Roerdink et al., 2016). Microbial sulfate reduction may have played a major role in these cases. In contrast, sediment-hosted pyrite analyzed by Montinaro et al. (2015) exhibits positive $\Delta^{33}S$ and $\delta^{34}S$ compositions, which they attributed to the incorporation of photolytic elemental sulfur; that is, a process independent of sulfate reduction. A wide range of $\delta^{34}S$ and $\Delta^{33}S$ values was obtained by Grosch et al. (2023) for pyrites from silicified volcanosedimentary rocks of the ca. 3.45 to 3.33 Ga Onverwacht Group in the Barberton greenstone belt. Chert-hosted pyrite from the Kromberg Formation records positive S-MIF signatures (up to +2‰ $\Delta^{33}S$) and negative $\delta^{34}S$ values (–8.25 to –0.9‰), which these authors interpreted to be a result of microbial disproportionation of elemental sulfur. Significant atmospheric sulfur components are reflected by the positive S-MIF signatures of the HC2 chert unit in the Hooggenoeg Formation ($\Delta^{33}S$ of up to +3.42‰ and $\delta^{34}S$ of up to +3‰; Grosch et al., 2023).

Our sulfide ore sulfur isotope data expand on available data for Paleoarchean greenstone belts. At first glance, the observed S-MIF signature of $\Delta^{33}S$ = –0.53‰ suggests involvement of a sedimentary sulfate (e.g., barite) component that was incorporated into hydrothermal fluids. However, Archean barite typically has large positive $\delta^{34}S$ values, which have not been measured for the Nondweni sulfides. Thus, the most plausible explanation for the observed S-MIF signature at negative $\delta^{34}S$ values is incorporation of surficial sulfur from altered sea-floor sources (Alt and Shanks, 2011; Evans et al., 2014), which were scavenged for their base metals and sulfur during sea-floor hydrothermal activity in an active back-arc spreading environment.

Genesis of the 3.52 to 3.45 Ga komatiitic basalts and basalts in the Nondweni greenstone belt

Element mobility: Archean mafic-ultramafic volcanic rocks have undergone postemplacement hydrothermal alteration and metamorphism, which results in the mobilization of certain chemical elements. It is therefore important to investigate the extent of major and trace element mobility before addressing the classification and petrogenesis of these rocks. Previous studies suggested that some of the metavolcanic rocks in the Nondweni greenstone belt have undergone some degree of silicification, which is especially relevant to pillowed basalts (Hofmann and Wilson, 2007). Silicification and other forms of metasomatic overprinting result typically in the mobility of Rb, Sr, Cs, Ba, K, Na, Ca, and Fe (Condie et al., 1977). In contrast, Al, Ti, Cr, Ni, Sc, V, Nb, Ta, Zr, Hf, Th, Y, and the HREEs are less affected by alteration and metamorphism. These relatively immobile elements can therefore be used in geochemical rock classifications and for petrogenetic interpretations.

Variation diagrams of TiO_2, Nb, Sm, and Gd versus Zr show consistency, which according to Polat and Hofmann (2003) attests to the immobile behavior of these elements (App. Fig. A14). Furthermore, a plot of Na_2O versus MgO is used to establish that only minimal alteration has affected the mafic-ultramafic rocks studied because there is no deviation from the negative trend typically observed for pristine volcanic rocks (App. Fig. A14). In the absence of strong modifications of the concentrations and distributions of these elements in the mafic-ultramafic rocks from the Nondweni greenstone belt, they can be used to constrain the origin and evolution of these mantle-sourced magmas, but only after an assessment of the effects of crustal contamination.

Effects of crustal contamination: Controversy exists about whether Early Archean "greenstones" erupted and evolved in an oceanic setting (Anhaeusser, 1975; de Wit et al., 1987a, b, 2011; Furnes et al., 2011, 2013; Xie et al., 2012; Bolhar et al., 2021; Wilson and Riganti, 2022) or were emplaced subaqueously onto an even older buried granitoid basement (Kröner et al., 1991, 1996, 2013; Grosch et al., 2011). In the latter scenario, there is high potential for magma contamination by felsic crustal materials (Campbell and Davies, 2017). The chemical compositions of greenstone successions and their zircon inventory have shown that preexisting granitoid basement was occasionally involved in their petrogenesis, albeit only to small extents. For example, in the Barberton greenstone belt, zircon records have yielded approximately 3.7-b.y.-old xenocrysts within the 3.45 Ga Vlakplaats granodiorite that intrudes the greenstones of the ca. 3.53 Ga Theespruit Formation (Schneider et al., 2019, and references therein). In the Kambalda-Norseman greenstone belts of Western Australia, older zircon xenocrysts from a buried gneissic basement were recovered from Paleoarchean volcanic rocks (Compston et al., 1986).

For the Nondweni greenstone belt, it has been shown that the mafic lavas are characterized by limited contamination with felsic materials along with limited fractional crystallization (Wilson and Riganti, 2022). The most probable contaminants of the mafic lavas were identified to be granitoids from the ca. 3.6 Ga Ancient Gneiss Complex, which has limited surface exposures north of the Nondweni greenstone belt in Eswatini (formerly known as Swaziland) but has been inferred to form part of a regionally extensive Early Archean migmatitic basement across the eastern Kaapvaal craton (Wilson and Riganti, 2022). Mixing calculations using samples from the Ancient Gneiss Complex suggest 5 to 10% contamination of the high-Ti and low-Ti basaltic lavas from the Paleoarchean Nondweni greenstone belt (Wilson and Riganti, 2022). This estimate of the degree of contamination is much smaller than that reported for Paleoarchean greenstones from Barberton, where 15 to 25% assimilation + fractional crystallization or 30% contamination by the Ancient Gneiss Complex have been suggested (Schneider et al., 2019).

To check for crustal contamination of our mafic-ultramafic metavolcanic rock samples, we use the Th/Yb versus Nb/Yb discrimination diagram (App. Fig. A15; Pearce, 2008). We note that the basaltic samples fall slightly above the modern MORB-ocean island basalt (OIB) array. The highest Th/Yb (0.55–0.72) and Nb/Yb (3.75) values occur in the low-Ti basalt group, whereas the high-Ti basalt group is characterized by slightly lower Th/Yb (0.38–0.42) and Nb/Yb (1.99–2.39). The komatiitic basalts have very low Nb/Yb (0.36–0.58) and Th/Yb (0.04–0.05) ratios. They fall within the MORB-OIB array, close to depleted mantle compositions, which suggests a strongly depleted mantle source. This also suggests different mantle sources for the basalts and komatiitic basalts; however, the high Th and low Nb contents of the basaltic samples may indicate input from continental crust-derived materials.

Downloaded from http://pubs.geoscienceworld.org/segweb/economicgeology/article-pdf/120/4/903/7306681/5162_netshidzivhe_et_al.pdf
by The Lib. East China Geol Inst. user

Such Th enrichment is absent from the komatiitic basalts and highlights differences in the petrogenesis of the two volcanic rock suites.

In a TiO_2/Yb versus Th/Nb diagram, the basaltic samples fall within the field for continental crust, although a few low-Ti samples overlap with the enriched mantle (EM)-OIB field (App. Fig. A15). The komatiitic basalts have very low TiO_2/Yb and Th/Nb ratios falling within the MORB + oceanic plateau basalt (OPB) field, close to depleted mantle values. The two diagrams in Appendix Figure A15 suggest that the basaltic rocks from the Nondweni greenstone belt record involvement of a continental crust-derived component, as was also identified by Wilson and Riganti (2022) for different samples. Primitive mantle is characterized by normalized La/Sm of 1 and Nb/Th of 8, and any mantle-derived magma that was contaminated by the continental crust upon ascent will show >1 La/Sm and <8 Nb/Th (Sun and McDonough, 1989; Rudnick and Gao, 2004). Conversely, uncontaminated basaltic magmas typically show La/Sm values close to 1 and Nb/Th ratios of ≥8 (Xie et al., 1993; Kerrich and Xie, 2002; Wyman and Kerrich, 2009; Said et al., 2012). For the Nondweni greenstone belt, the low-Ti basalt (1.67–2 $[La/Sm]_N$), high-Ti basalt (1.42–1.69), and komatiitic basalt (1.47–2.6) samples reveal significant variations in La/Sm. Nb/Th is highest in the komatiitic basalts ranging between 8 and 12, whereas this ratio is <8 for the basaltic samples. These values reconcile with the relatively low levels of crustal contamination proposed for the basaltic samples studied here, and also those analyzed by Wilson and Riganti (2022).

Origins of the komatiitic basalts and associated mafic volcanic rocks: The major and trace element compositions of mafic-ultramafic volcanic rocks provide clues to the compositions and locations of their mantle sources. There is increasing evidence for the operation of plate tectonics during the Early Archean (and possibly prior), and researchers studying the geochemistry of mafic-ultramafic lavas in Paleoarchean greenstone belts have identified fingerprints from all major plate tectonic environments, such as mid-ocean ridges, back-arc basins, and intraoceanic arcs (i.e., subduction zones), but also signatures diagnostic of mantle plumes (e.g., Smithies et al., 2005a; Herzberg et al., 2010; Bédard, 2013). Komatiites are a volumetrically minor but highly significant component of the volcanic record of Archean greenstone belts (<5%; de Wit and Ashwal, 1995). Importantly, komatiites sensu stricto are absent in the Paleoarchean Nondweni greenstone belt. The occurrence of metavolcanic rocks with pyroxene spinifex textures suggests that the petrogenesis (e.g., magma sources and temperatures) of the Nondweni greenstone belt "komatiitic basalts" differs from that of bona fide olivine spinifex-textured komatiites found in most Archean greenstone belts worldwide, such as in Barberton and Buffalo River in South Africa, Abitibi in Canada, Pilbara in Australia, Rio das Velhas in Brazil, and Badampahar in India (Robin-Popieul et al., 2012; van Acken et al., 2016; Ghosh et al., 2019; Netshidzivhe et al., 2023). This observation is also illustrated by the higher silica content of the mafic-ultramafic volcanic rocks from the Nondweni greenstone belt (up to 56 wt % SiO_2) when compared to equivalent rocks from other greenstone belts on the Kaapvaal craton (Hofmann et al., 2019). Another rare example of the occurrence of pyroxene spinifex-textured lava flows without an association with olivine spinifex-textured komatiites is the Murchison domain of the Yilgarn craton in Western Australia (Lowrey et al., 2017).

The variation in the geochemical composition of the mafic-ultramafic volcanic rocks from the Nondweni greenstone belt suggests the existence of three discrete magmatic groups: high-Ti basalts, low-Ti basalts, and komatiitic basalts (of boninitic affinity). Although the classification of primitive metavolcanic rocks based on their Al_2O_3/TiO_2 ratios is intended for bona fide komatiites (e.g., Robin-Popieul et al., 2012), application of this scheme to the mafic-ultramafic rocks from the Nondweni greenstone belt identifies Al-depleted basalts and Al-enriched komatiitic basalts. The Al-depleted basalts show LREE enrichment with subchondritic Al_2O_3/TiO_2 ratios (9–11). The high-Ti and low-Ti basalt groups show slight variations in their trace element characteristics (App. Fig. A8), which may point to magma origins from different mantle sources at different depths or from the same peridotitic source with different degrees of partial melting. Coexistence of high-Ti and low-Ti basalts within a single volcanic succession is common in Phanerozoic large igneous provinces (LIPs) such as the Karoo LIP in Africa-Antarctica and the Emeishan LIP in Central Asia (Jourdan et al., 2007; Shao et al., 2022). The most widely accepted explanation for this dichotomy is involvement of discrete mantle source components that contribute to the partial melts at different depths (Marsh et al., 2001; Ernst, 2014; Heinonen et al., 2022; Zhang et al., 2022; Tappe et al., 2023). We note that the most primitive basalts in the Nondweni greenstone belt have 8 to 12 wt % MgO at low TiO_2 (0.8–1.1 wt %). Such melts may be generated at high pressures by moderate degrees of partial melting (15–20%) of a peridotitic source in the garnet stability field. The HREE depletion [average $(Gd/Yb)_N$ = 1.45] of these basalts further indicates a garnet control during partial melting (Smithies et al., 2005b; Pearce et al., 2021).

Komatiites and komatiitic basalts of boninitic affinity are identified in most greenstone belts worldwide (Pearce and Reagan, 2019). The presence of boninite-like geochemical signatures in the 3.52- to 3.45-b.y.-old komatiitic basalts of the Witkop Formation in the Nondweni greenstone belt is significant and warrants an explanation. These rocks are distinguished from the associated tholeiitic basalts and basaltic andesites mainly by their higher MgO (>12 wt %) and lower TiO_2 (<0.2 wt %) and SiO_2 (~52 wt %) contents. They have very low Nb contents between 0.49 and 0.83 ppm, <1 $(Gd/Yb)_N$, and Al_2O_3/TiO_2 between 53 and 59. Modern boninites are closely linked to volcanism following subduction initiation in intraoceanic arc and forearc environments (Kerrich et al., 1998; Polat et al., 2002; Smithies et al., 2004; Stern et al., 2012; Turner et al., 2014; Lowrey et al., 2019; Pearce and Reagan, 2019). Hence, identification of boninitic rocks (also referred to as boninite-like) in Paleoarchean greenstone belts may provide additional evidence for the operation of subduction zones as early as 3.5 b.y. ago (Smithies et al., 2004). However, it is important to note that although a boninite-like character of the komatiitic basalts from the Nondweni greenstone belt is apparent from their major element compositions (App. Fig. A8), their trace element systematics do not show boninite affinity (App. Fig. A8). The four komatiitic basalt

Downloaded from http://pubs.geoscienceworld.org/segweb/economicgeology/article-pdf/120/4/903/7306681/5162_netshidzivhe_et_al.pdf
by The Lib, East China Geol Inst. user

samples analyzed fall within the MORB-OIB array in the Th/Yb versus Nb/Yb diagram, and they do not extend into the arc field (App. Fig. A15). We argue that these trace element systematics deviate significantly from those of true boninites (App. Fig. A8; Li et al., 2013) and, thus, the komatiitic basalts do not support the operation of subduction in the Nondweni greenstone belt by ca. 3.5 Ga.

In their review of Archean boninites, Smithies et al. (2004) discussed two key localities referred to as Whundo-type and Whitney-type boninites. The ca. 3.4 Ga Whundo-type lava flows in the Pilbara craton of Western Australia were found to be geochemically similar to Cenozoic boninites. This similarity refers to their strongly enriched overlapping LREE and Th concentrations, which is ascribed to mobility of subduction zone fluids that reenriched the ultradepleted shallow mantle wedge sources of boninites in slab-derived components, including those derived from pelagic sediment (Kerrich et al., 1998; Boily and Dion, 2002; Polat et al., 2002; Smithies, 2002). In contrast, the ca. 2.7 Ga Whitney-type lava flows in the Abitibi belt of eastern Canada are LREE depleted and HREE enriched compared to the Whundo-type lavas. These tend to be much more aluminous and have no pronounced negative Nb and Ti anomalies (Kerrich et al., 1998). The Whitney-type boninites are spatiotemporally associated with mantle plume-derived komatiites and tholeiitic basalts (Kerrich et al., 1998). Importantly, we note that the komatiitic basalts of the Nondweni greenstone belt are geochemically quite similar to the Whitney-type boninites from the Abitibi belt. Similar boninite-like melts are represented by the ca. 3.3 Ga ultradepleted, Al-enriched komatiites in the Commondale greenstone belt on the eastern Kaapvaal craton (Wilson, 2002, 2003, 2019). We therefore argue that such boninite-like komatiitic magmas may have formed by moderately high degrees of partial melting of a strongly depleted refractory peridotitic mantle source at relatively shallow depths, but only after some reenrichment in incompatible elements had occurred, which was not necessarily linked to subduction zone processes.

Conclusions

High-precision CA-ID-TIMS U/Pb zircon geochronology provides evidence for submarine rhyolite volcanism as part of the Nondweni greenstone belt succession at 3531.91 ± 0.46 Ma. These Paleoarchean rhyolites are the immediate host rocks to a Zn-Cu-Pb-Ag VMS-type mineralization in the Toggekry Formation at the southern Kaapvaal craton margin. The massive sulfide occurrence is referred to as the St. James deposit and possibly presents the world's oldest preserved VMS mineralization.

REE modeling suggests that the association of tholeiitic basalts and rhyolites in the Paleoarchean Nondweni greenstone belt can be explained by moderate degrees of partial melting (12–17%) of hydrothermally altered basaltic material at shallow depth within hot oceanic crust. The multiple sulfur isotope compositions of the tholeiitic basalts record unfractionated $\delta^{34}S$ and $\Delta^{33}S$ signatures, suggesting a purely magmatic sulfur source. The $\delta^{34}S$ values of the rhyolites resemble those of seawater-altered basaltic oceanic crust, which supports the proposed link between these rock types via partial melting. The attenuated $\Delta^{33}S$ compositions of the rhyolites do not reveal an S-MIF signature, which excludes significant input of sediment-sourced sulfur during local partial melting of the Paleoarchean oceanic crust.

The rhyolite-hosted base metal sulfide mineralization at the St. James site exhibits notably negative $\Delta^{33}S$, which defines a fully resolved S-MIF signature. The S-MIF signature is best ascribed to a contribution of surficial sulfur component into the magmatic-hydrothermal fluids that circulated through the oceanic crust in an active back-arc setting. Our preferred model for VMS deposit formation in a back-arc rift environment at ca. 3.53 Ga assumes the operation of subduction zone processes. For the Kaapvaal craton, this inference aligns with evidence from Archean placer diamonds that sampled >3.5-b.y.-old crustal components from >150-km depth, which is best explained by some form of early plate tectonics.

Acknowledgments

This study is a part of the PhD thesis by TN, who received funding from the National Research Foundation of South Africa (NRF). ST acknowledges funding from the NRF provided by the IPRR grant program and CIMERA. Parts of the analytical costs for this project were covered with DSI-NRF SARChI funds, awarded to FV. We thankfully acknowledge help from the following colleagues: Azhar Shaikh (field companionship), Henriette Ueckermann (LA-MC-ICP-MS support), Christian Reinke (EPMA and XRF support), and the late Roger Dixon for help with the SELFRAG equipment. This study benefited from discussions with Andrea Agangi, Kris Szilas, and Elis Hoffmann. We would like to express our gratitude to the reviewers, David Huston and Stefanie Brueckner, and to the editor, David Cooke, for highly constructive feedback.

REFERENCES

Alt, J.C., 1994, A sulfur isotopic profile through the Troodos ophiolite, Cyprus: Primary composition and the effects of seawater hydrothermal alteration: Geochimica et Cosmochimica Acta, v. 58, p. 1825–1840.

——1995, Sub-seafloor processes in mid-ocean ridge hydrothermal systems: American Geophysical Union Monograph, v. 91, p. 85–114.

Alt, J.C., and Shanks, W.C., 2011, Microbial sulfate reduction and the sulfur budget for a complete section of altered oceanic basalts, IODP Hole 1256D (eastern Pacific): Earth and Planetary Science Letters, v. 310, p. 73–83.

Anhaeusser, C.R., 1975, Precambrian tectonic environments: Annual Review of Earth and Planetary Sciences, v. 3, p. 31–53.

Aoyama, S., and Ueno, Y., 2018, Multiple sulfur isotope constraints on microbial sulfate reduction below an Archean seafloor hydrothermal system: Geobiology, v. 16, p. 107–120.

Arndt, N.T., and Fleet, M.E., 1979, Stable and metastable pyroxene crystallization in layered komatiite lava flows: American Mineralogist, v. 64, p. 856–864.

Arndt, N.T., Lesher, M.C., and Barnes, S.J., 2008, Komatiite: Cambridge, Cambridge University Press, 487 p.

Barker, F., 1979, Trondhjemite: Definition, environment and hypotheses of origin, *in* Barker, F., ed., Trondhjemites, dacites and related rocks: Amsterdam, Elsevier, p. 1–11.

Barnes, S.J., and Arndt, N.T., 2019, Distribution and geochemistry of komatiites and basalts through the Archean, *in* Van Kranendonk, M.J., Bennett, V.C., and Hoffmann, J.E., eds., Earth's oldest rocks: Elsevier, p. 103–132.

Barrie, C.T., and Hannington, M.D., 1999, Classification of VMS deposits based on host rock composition: Reviews in Economic Geology, v. 8, p. 1–11.

Bao, H., Rumble, D., III, and Lowe, D.R., 2007, The five stable isotope compositions of Fig Tree barites: Implications on sulfur cycle in ca. 3.2 Ga oceans: Geochimica et Cosmochimica Acta, v. 71, p. 4868–4879.

Bédard, J.H., 2013, How many arcs can dance on the head of a plume?: A 'Comment' on: "A critical assessment of Neoarchean 'plume only' geodynamics: Evidence from the Superior province, by Derek Wyman, Precambrian Research": Precambrian Research, v. 229, p. 189–197.

Downloaded from http://pubs.geoscienceworld.org/segweb/economicgeology/article-pdf/120/4/903/7306681/5162_netshidzivhe_et_al.pdf
by The Lib. East China Geol Inst. user

Binns, R.A., and Scott, S.D., 1993, Actively forming polymetallic sulfide deposits associated with felsic volcanic rocks in the eastern Manus back-arc basin, Papua New Guinea: Economic Geology, v. 88, p. 2226–2236.
Boily, M., and Dion, C., 2002, Geochemistry of boninite-type volcanic rocks in the Frotet-Evans greenstone belt, Opatica subprovince, Quebec: Implications for the evolution of Archaean greenstone belts: Precambrian Research, v. 115, p. 349–371.
Bolhar, R., Tappe, S., Wilson, A.H., et al., 2021, A petrochronology window into near-surface fluid/rock interaction within Archaean ultramafic-mafic crust: Insights from the 3.25 Ga Stolzburg Complex, Barberton greenstone belt: Chemical Geology, v. 569, article 120130.
Burness, S., Thomassot, E., Smart, K.A., and Tappe, S., 2021, Sulfur isotopes ($\delta^{34}S$ and $\Delta^{33}S$) in sulfides from cratonic mantle eclogites: A glimpse of volatile cycling in ancient subduction zones: Earth and Planetary Science Letters, v. 572, p. 1–12.
Carmichael, I.S.E., 1964, The petrology of Thingmuli, a Tertiary volcano in eastern Iceland: Journal of Petrology, v. 5, p. 435–460.
Campbell, I.H., and Davies, D.R., 2017, Raising the continental crust: Earth and Planetary Science Letters, v. 460, p. 112–122.
Campbell, I.H., Franklin, J.M., Gorton, M.P., Hart, T.R., and Scott, S.D., 1981, The role of subvolcanic sills in the generation of massive sulfide deposits: Economic Geology, v. 76, p. 2248–2253.
Candela, P.A., 2003, Ores in the Earth's crust, *in* Holland, H.D., and Turekian, K.K., eds., Treatise on geochemistry: Elsevier, p. 411–431.
Cathles, L.M., Erendi, A.H.J., and Barrie, T.J.E.G., 1997, How long can a hydrothermal system be sustained by a single intrusive event?: Economic Geology, v. 92, p. 766–771.
Cawood, P.A., and Hawkesworth, C.J., 2015, Temporal relations between mineral deposits and global tectonic cycles: The Geological Society of London, Special Publication 393, p. 9–21.
Compston, W., Williams, I.S., Campbell, I.H., and Gresham, J.J., 1986, Zircon xenocrysts from the Kambalda volcanics: Age constraints and direct evidence for older continental crust below the Kambalda-Norseman greenstones: Earth and Planetary Science Letters, v. 76, p. 299–311.
Condie, K.C., Viljoen, M.J., and Kable, E.J.D., 1977, Effects of alteration on element distributions in Archean tholeiites from the Barberton greenstone belt, South Africa: Contributions to Mineralogy and Petrology, v. 64, p. 75–89.
Condomines, M., Grönvold, K., Hooker, P.J., et al., 1983, Helium, oxygen, strontium and neodymium isotopic relationships in Icelandic volcanics: Earth and Planetary Science Letters, v. 66, p. 125–136.
Crawford, A.J., Falloon, T.J., and Green, D.H., 1989, Classification, petrogenesis and tectonic setting of boninites, *in* Crawford, A.J, ed., Boninites and related rocks: Allen and Unwin, Australia, p. 1–49.
de Ronde, C.E., and de Wit, M.J., 1994, Tectonic history of the Barberton greenstone belt, South Africa: 490 million years of Archean crustal evolution: Tectonics, v. 13, p. 983–1005.
de Wit, M.J., 2004, Archean greenstone belts do contain fragments of ophiolites: Developments in Precambrian Geology, v. 13, p. 599–614.
de Wit, M.J., and Ashwal, L.D., 1995, Greenstone belts: What are they?: South African Journal of Geology, v. 98, p. 505–520.
de Wit, M.J, Hart, R.A., and Hart, R., 1987a, The Jamestown Ophiolite Complex, Barberton mountain belt: A section through 3.5 Ga oceanic crust: Journal of African Earth Sciences, v. 6, p. 681–730.
de Wit, M.J., Armstrong, R., Hart, R.J., and Wilson, A.H., 1987b, Felsic igneous rocks within the 3.3 to 3.5 Ga Barberton greenstone belt: High crustal level equivalents of the surrounding tonalite-trondhjemite terrain, emplaced during thrusting: Tectonics, v. 6, p. 529–549.
de Wit, M.J., Furnes, H., and Robins, B., 2011, Geology and tectonostratigraphy of the Onverwacht Suite, Barberton greenstone belt, South Africa: Precambrian Research, v. 186, p. 1–27.
Ernst, R.E., 2014, Large igneous provinces: Cambridge, Cambridge University Press, 653 p.
Ersoy, E.Y., 2013, PETROMODELER (Petrological Modeler): A Microsoft® Excel© spreadsheet program for modelling melting, mixing, crystallization and assimilation processes in magmatic systems: Turkish Journal of Earth Sciences, v. 22, p. 115–125.
Evans, K.A., Tomkins, A.G., Cliff, J., and Fiorentini, M.L., 2014, Insights into subduction zone sulfur recycling from isotopic analysis of eclogite-hosted sulfides: Chemical Geology, v. 365, p. 1–19.
Farquhar, J., and Wing, B.A., 2003, Multiple sulfur isotopes and the evolution of the atmosphere: Earth and Planetary Science Letters, v. 213, p.1–13.
Farquhar, J., Bao, H., and Thiemens, M., 2000, Atmospheric influence of Earth's earliest sulfur cycle: Science, v. 289, p. 756–758.
Farquhar, J., Wing, B.A., McKeegan, K.D., et al., 2002, Mass-independent sulfur of inclusions in diamond and sulfur recycling on early Earth: Science, v. 298, p. 2369–2372.
Farquhar, J., Wu, N., Canfield, D.E., and Oduro, H., 2010, Connections between sulfur cycle evolution, sulfur isotopes, sediments, and base metal sulfide deposits: Economic Geology, v. 105, p. 509–533.
Fouquet, Y., Cambon, P., Etoubleau, J., et al., 2010, Geodiversity of hydrothermal processes along the Mid-Atlantic Ridge and ultramafic-hosted mineralization: A new type of oceanic Cu-Zn-Co-Au volcanogenic massive sulfide deposit: American Geophysical Union, Geophysical Monograph Series, no. 188, p. 321–367.
Fowler, A.D., Jensen, L.S., and Peloquin, S.A., 1987, Varioles in Archean basalts: Products of spherulitic crystallization: The Canadian Mineralogist, v. 25, p. 275–289.
Fowler, A.D., Berger, B., Shore, M., Jones, M.I., and Ropchan, J., 2002, Supercooled rocks: Development and significance of varioles, spherulites, dendrites and spinifex in Archean volcanic rocks, Abitibi greenstone belt, Canada: Precambrian Research, v. 115, p. 311–328.
Franklin, J.M., Sangster, D.M., and Lydon, J.W., 1981, Volcanic-associated massive sulfide deposits: Economic Geology, 75th Anniversary Volume, p. 485–627.
Franklin, J.M., Gibson, H.L., Jonasson, I.R. and Galley, A.G., 2005, Volcanogenic massive sulfide deposits: Economic Geology, 100th Anniversary Volume, p. 523–560.
Furman, T., Meyer, P.S., and Frey, F., 1992, Evolution of Icelandic central volcanoes: Evidence from the Austurhorn intrusion, southeastern Iceland: Bulletin of Volcanology, v. 55, p. 45–62.
Furnes, H.D., de Wit, M.J., Robins, B., and Sandstå, N.R., 2011, Volcanic evolution of the upper Onverwacht Suite, Barberton greenstone belt, South Africa: Precambrian Research, v. 186, p. 28–50.
Furnes, H.D., De Wit, M., and Robins, B., 2013, A review of new interpretations of the tectonostratigraphy, geochemistry and evolution of the Onverwacht Suite, Barberton greenstone belt, South Africa: Gondwana Research, v. 23, p. 403–428.
Galley, A.G., 1993, Characteristics of semi-conformable alteration zones associated with volcanogenic massive sulfide districts: Journal of Geochemical Exploration, v. 48, p. 175–200.
——2003, Composite synvolcanic intrusions associated with Precambrian VMS-related hydrothermal systems: Mineralium Deposita, v. 38, p. 443–473.
Galley, A.G., Hannington, M.D., and Jonasson, I.R., 2007, Volcanogenic massive sulfide deposits: Geological Association of Canada, Mineral Deposits Division, Special Publication 5, p. 141–161.
Gélinas, L., Brooks, C., and Trzcienski, W.E., Jr., 1976, Archean variolites—quenched immiscible liquids: Canadian Journal of Earth Sciences, v. 13, p. 210–230.
Ghosh, R., Vermeesch, P., Gain, D., and Mondal, R., 2019, Genetic relationship among komatiites and associated basalts in the Badampahar greenstone belt (3.25-3.10 Ga), Singhbhum craton, eastern India: Precambrian Research, v. 327, p. 196–211.
Grosch, E.G., Kosler, J., McLoughlin, N., et al., 2011, Paleoarchean detrital zircon ages from the earliest tectonic basin in the Barberton greenstone belt, Kaapvaal craton, South Africa: Precambrian Research, v. 191, p. 85–99.
Grosch, E.G., McLoughlin, N., and Whitehouse, M., 2023, Multiple sulfur isotope record of Paleoarchean sedimentary rocks across the Onverwacht Group, Barberton greenstone belt, South Africa: Geobiology, v. 2, p. 153–167.
Hannington, M.D., 2014, Volcanogenic massive sulfide deposits, *in* Holland, H.D., and Turekian, K.K., eds., Treatise on geochemistry, 2nd ed.: Elsevier, p. 463–488.
Heinonen, J.S., Brown, E.L., Turunen, S.T., and Luttinen, A.V., 2022, Heavy rare earth elements and the sources of continental flood basalts: Journal of Petrology, v. 63, article egac098.
Herzberg, C., Condie, K., and Korenaga, J., 2010, Thermal history of the Earth and its petrological expression: Earth and Planetary Science Letters, v. 292, p. 79–88.
Hickey, R.L., and Frey, F.A., 1982, Geochemical characteristics of boninite series volcanics: Implications for their source: Geochimica et Cosmochimica Acta, v. 46, p. 2099–2115.
Hickman, A.H., 2023, Archean evolution of the Pilbara craton and Fortescue basin: Springer Nature, 510 p.
Hickman, A.H., and Van Kranendonk, M.J., 2008, Archean crustal evolution and mineralization of the northern Pilbara craton: A field guide: Geological Survey of Western Australia, Record 2008/13.

Downloaded from http://pubs.geoscienceworld.org/segweb/economicgeology/article-pdf/120/4/903/7306681/5162_netshidzivhe_et_al.pdf
by The Lib. East China Geol Inst. user

Hofmann, A., and Wilson, A.H., 2007, Silicified basalts, bedded cherts and other seafloor alteration phenomena of the 3.4 Ga Nondweni greenstone belt, South Africa: Developments in Precambrian Geology, v. 15, p. 571–605.
Hofmann, A., Bolhar, R., Orberger, B., and Foucher, F., 2013, Cherts of the Barberton greenstone belt, South Africa: Petrology and trace-element geochemistry of 3.5 to 3.3 Ga old silicified volcaniclastic sediments: South African Journal of Geology, v. 116, p. 297–322.
Hofmann, A., Anhaeusser, C.R., Dixon, J., et al., 2019, Archaean granitoid-greenstone geology of the southeastern part of the Kaapvaal craton, *in* Kröner, A., and Hofmann, A., eds., The Archaean geology of the Kaapvaal craton, Southern Africa: Springer, p. 33–54.
Hollis, S.P., Yeats, C.J., Wyche, S., et al., 2015, A review of volcanic-hosted massive sulfide (VHMS) mineralization in the Archaean Yilgarn craton, Western Australia: Tectonic, stratigraphic and geochemical associations: Precambrian Research, v. 260, p. 113–135.
Hoskin, P.W.O., and Ireland, T.R., 2000, Rare earth element chemistry of zircon and its use as a provenance indicator: Geology, v. 28, p. 627–630.
Huston, D.L., Morant, P., Pirajno, F., et al., 2007, Paleoarchean mineral deposits of the Pilbara craton: Genesis, tectonic environment and comparisons with younger deposits: Developments in Precambrian Geology, v. 15, p. 411–450.
Huston, D.L., Pehrsson, S., Eglington, B.M., and Zaw, K., 2010, The geology and metallogeny of volcanic-hosted massive sulfide deposits: Variations through geologic time and with tectonic setting: Economic Geology, v. 105, p. 571–591.
Huston, D.L., Trumbull, R.B., Beaudoin, G., and Ireland, T., 2023, Light stable isotopes (H, B, C, O and S) in ore studies—methods, theory, applications and uncertainties, *in* Huston, D.L., and Gutzmer, J., eds., Isotopes in economic geology, metallogenesis and exploration: Springer, p. 209–244.
Jele, N., 2013, The genesis of the quartz sericite schists of the Toggekry Formation, Nondweni greenstone belt, South Africa: M.Sc. thesis, Durban, South Africa, University of KwaZulu-Natal, 191 p.
Johnston, D.T., 2011, Multiple sulfur isotopes and the evolution of Earth's surface sulfur cycle: Earth-Science Reviews, v. 106, p. 161–183.
Jónasson, K., 1994, Rhyolite volcanism in the Krafla central volcano, northeast Iceland: Bulletin of Volcanology, v. 56, p. 516–528.
Jourdan, F., Féraud, G., Bertrand, H., Watkeys, M.K., and Renne, P.R., 2007, Distinct brief major events in the Karoo large igneous province clarified by new $^{40}Ar/^{39}Ar$ ages on the Lesotho basalts: Lithos, v. 98, p. 195–209.
Kalender, L., 2011, Oxygen, carbon and sulfur isotope studies in the Keban Pb-Zn deposits, eastern Turkey: An approach on the origin of hydrothermal fluids: Journal of African Earth Sciences, v. 59, p. 341–348.
Kerrich, R., and Xie, Q., 2002, Compositional recycling structure of an Archean super-plume: Nb-Th-U-LREE systematics of Archean komatiites and basalts revisited: Contributions to Mineralogy and Petrology, v. 142, p. 476–484.
Kerrich, R., Wyman, D., Fan, J., and Bleeker, W., 1998, Boninite series: Low-Ti tholeiite associations from the 2.7 Ga Abitibi greenstone belt: Earth and Planetary Science Letters, v. 164, 303–316.
Kröner, A., Byerly, G.R., and Lowe, D.R., 1991, Chronology of early Archaean granite-greenstone evolution in the Barberton Mountain Land, South Africa, based on precise dating by single zircon evaporation: Earth and Planetary Science Letters, v. 103, p. 41–54.
Kröner, A., Hegner, E., Wendt, J.I., and Byerly, G.R., 1996, The oldest part of the Barberton granitoid-greenstone terrain, South Africa: Evidence for crust formation between 3.5 and 3.7 Ga: Precambrian Research, v. 78, p. 105–124.
Kröner, A., Hoffmann, J. E., Xie, H. Q., et al., 2013, Generation of early Archaean felsic greenstone volcanic rocks through crustal melting in the Kaapvaal craton, southern Africa: Earth and Planetary Science Letters, v. 381, p. 188–197.
Labidi, J., Cartigny, P., Birck, J.L., Assayag, N., and Bourrand, J.J., 2012, Determination of multiple sulfur isotopes in glasses: A reappraisal of the MORB $\delta^{34}S$: Chemical Geology, v. 334, p. 189–198.
Labidi, J., Cartigny, P., and Moreira, M., 2013, Non-chondritic sulphur isotope composition of the terrestrial mantle: Nature, v. 501, p. 208–211.
Labidi, J., Cartigny, P., Hamelin, C., Moreira, M., and Dosso, L., 2014, Sulfur isotope budget (^{32}S, ^{33}S, ^{34}S and ^{36}S) in Pacific–Antarctic ridge basalts: A record of mantle source heterogeneity and hydrothermal sulfide assimilation: Geochimica et Cosmochimica Acta, v. 133, p. 47–67.
LaFlamme, C., Jamieson, J.W., Fiorentini, M.L., et al., 2018, Investigating sulfur pathways through the lithosphere by tracing mass independent fractionation of sulfur to the Lady Bountiful orogenic gold deposit, Yilgarn craton: Gondwana Research, v. 58, p. 27–38.
Laurent, O., Björnsen, J., Wotzlaw, J.F., et al., 2020, Earth's earliest granitoids are crystal-rich magma reservoirs tapped by silicic eruptions: Nature Geoscience, v. 13, p. 163–169.
Lentz, D.R., 1998, Petrogenetic evolution of felsic volcanic sequences associated with Phanerozoic volcanic-hosted massive sulfide systems: The role of extensional geodynamics: Ore Geology Reviews, v. 12, p. 289–327.
Lesher, C.M., Goodwin, A.M., Campbell, I.H., and Gorton, M.P., 1986, Trace-element geochemistry of ore-associated and barren, felsic metavolcanic rocks in the Superior Province, Canada: Canadian Journal of Earth Sciences, v. 23, p. 222–237.
Li, Y.B., Kimura, J.I., Machida, S., et al., 2013, High-Mg adakite and low-Ca boninite from a Bonin fore-arc seamount: Implications for the reaction between slab melts and depleted mantle: Journal of Petrology, v. 54, p. 1149–1175.
Lowe, D.R., 1994, Accretionary history of the Archean Barberton greenstone belt (3.55–3.22 Ga), southern Africa: Geology, v. 22, p. 1099–1102.
Lowrey, J.R., Ivanic, T.J., Wyman, D.A., and Roberts, M.P., 2017, Platy pyroxene: New insights into spinifex texture: Journal of Petrology, v. 58, p. 1671–1700.
Lowrey, J.R., Wyman, D.A., Ivanic, T.J., Smithies, R.H., and Maas, R., 2019, Archean boninite-like rocks of the Northwestern Youanmi Terrane, Yilgarn craton: Geochemistry and genesis: Journal of Petrology, v. 60, p. 2131–2168.
Lydon, J.W., 1984, Volcanogenic massive sulfide deposits Part I: A descriptive model: Geoscience Canada, v. 11, p. 195–202.
Macdonald, R., Sparks, R.S.J., Sigurdsson, H., et al., 1987, The 1875 eruption of Askja volcano, Iceland: Combined fractional crystallization and selective contamination in the generation of rhyolitic magma: Mineralogical Magazine, v. 51, p. 183–202.
Macdonald, R., McGarvie, D.W., Pinkerton, H., Smith, R.L., and Palacz, A., 1990, Petrogenetic evolution of the Torfajökull Volcanic Complex, Iceland I. Relationship between the magma types: Journal of Petrology, v. 31, p. 429–459.
MacLean, W.H., and Barrett, T.J., 1993, Lithogeochemical techniques using immobile elements: Journal of Geochemical Exploration, v. 48, p. 109–133.
Marsh, J.S., Ewart, A., Milner, S.C., Duncan, A.R. and Miller, R.M., 2001, The Etendeka Igneous Province: Magma types and their stratigraphic distribution with implications for the evolution of the Paraná-Etendeka flood basalt province: Bulletin of Volcanology, v. 62, p. 464–486.
Matthews, P.E., Charlesworth, E.G., Eglington, A.A., and Harmer, R.E., 1989, A minimum 3.29 Ga age for the Nondweni greenstone complex in the southeastern Kaapvaal craton: South African Journal of Geology, v. 92, p. 272–278.
McDonough, W.F., and Sun, S.S., 1995, The composition of the Earth: Chemical Geology, v. 120, p. 223–253.
McGarvie, D.W., Macdonald, R., Pinkerton, H., and Smith, R.L., 1990, Petrogenetic evolution of the Torfajökull volcanic complex, Iceland II. The role of magma mixing: Journal of Petrology, v. 31, p. 461–481.
Mercier-Langevin, P., Hannington, M.D., Dubé B., and Bécu, V., 2011, The gold content of volcanogenic massive sulfide deposits: Mineralium Deposita, v. 46, p. 509–539.
Mercier-Langevin, P., Gibson, H.G., Hannington, M.D., et al., 2014, A Special Issue on Archean magmatism, volcanism, and ore deposits: Part 2. volcanogenic massive sulfide deposits: Economic Geology, v. 109, p. 1–9.
Montinaro, A., Strauss, H., Mason, P.R., et al., 2015, Paleoarchean sulfur cycling: Multiple sulfur isotope constraints from the Barberton greenstone belt, South Africa: Precambrian Research, v. 267, p. 311–322.
Mungall, J.E., Brenan, J.M., Godel, B., Barnes, S.J., and Gaillard, F., 2015, Transport of metals and sulfur in magmas by flotation of sulfide melt on vapour bubbles: Nature Geoscience, v. 8, p. 216–219.
Nadeau, O., Williams-Jones, A.E., and Stix, J., 2010, Sulfide magma as a source of metals in arc-related magmatic hydrothermal ore fluids: Nature Geoscience, v. 3, p. 501–505.
Netshidzivhe, T., Tappe, S., Wilson, A.H., Ishikawa, A., and Viljoen, F., 2023, The Paleoarchean Buffalo River komatiites: Progressive melting of a single large mantle plume beneath the growing Kaapvaal craton: Precambrian Research, v. 393, article 107071.
Nicholson, H., Condomines, M., Fitton, J.G., et al., 1991, Geochemical and isotopic evidence for crustal assimilation beneath Krafla, Iceland: Journal of Petrology, v. 32, p. 1005–1020.
Nielsen, S.G., Rehkämper, M., Teagle, D.A., et al., 2006, Hydrothermal fluid fluxes calculated from the isotopic mass balance of thallium in the ocean crust: Earth and Planetary Science Letters, v. 251, p. 120–133.

Downloaded from http://pubs.geoscienceworld.org/segweb/economicgeology/article-pdf/120/4/903/7306681/5162_netshidzivhe_et_al.pdf
by The Lib. East China Geol Inst. user

Ohmoto, H., 1996, Formation of volcanogenic massive sulfide deposits: The Kuroko perspective: Ore Geology Reviews, v. 10, p. 135–177.
Óskarsson, N., Sigvaldason, G.E., and Steinthorsson, S., 1982, A dynamic model of rift zone petrogenesis and the regional petrology of Iceland: Journal of Petrology, v. 23, p. 28–74.
Óskarsson, N., Steinthorsson, S., and Sigvaldason, G.E., 1985, Iceland geochemical anomaly: Origin, volcanotectonics, chemical fractionation and isotope evolution of the crust: Journal of Geophysical Research: Solid Earth, v. 90, p. 10,011–10,025.
Patten, C.G.C., Pitcairn, I.K., Teagle., D.A.H., and Harris, M., 2016, Sulfide mineral evolution and metal mobility during alteration of the oceanic crust: Insights from ODP Hole 1256D: Geochimica et Cosmochimica Acta, v. 193, p. 132–159.
Pearce J.A., 1996, A user's guide to basalt discrimination diagrams: Geological Association of Canada, Short Course Notes, v. 12, p. 79–113.
——2008, Geochemical fingerprinting of oceanic basalts with applications to ophiolite classification and the search for Archean oceanic crust: Lithos, v. 100, p. 14–48.
Pearce, J.A., and Reagan, M. K., 2019, Identification, classification, and interpretation of boninites from Anthropocene to Eoarchean using Si-Mg-Ti systematics: Geosphere, v. 15, p. 1008–1037.
Pearce, J.A., Ernst, R.E., Peate, D.W., and Rogers, C., 2021, LIP printing: Use of immobile element proxies to characterize Large Igneous Provinces in the geologic record: Lithos, v. 392, article 106068.
Piercey, S.J., 2010, An overview of petrochemistry in the regional exploration for volcanogenic massive sulfide (VMS) deposits: Geochemistry: Exploration, Environment, Analysis, v. 10, p. 119–136.
Polat, A., and Hofmann, A.W., 2003, Alteration and geochemical patterns in the 3.7–3.8 Ga Isua greenstone belt, West Greenland: Precambrian Research, v. 126, p. 197–218.
Polat, A., Hofmann, A.W., and Rosing, M.T., 2002, Boninite-like volcanic rocks in the 3.7–3.8 Ga Isua greenstone belt, West Greenland: Geochemical evidence for intra-oceanic subduction zone processes in the early Earth: Chemical Geology, v. 184, p. 231–254.
Pyke, D.R., Naldrett, A.J., and Eckstrand O.R., 1973, Archean ultramafic flows in Munro Township, Ontario: Geological Society of America, Bulletin no. 84, p. 955–978.
Riganti, A., and Wilson, A.H., 1995, Geochemistry of the mafic/ultramafic volcanic associations of the Nondweni greenstone belt, South Africa, and constraints on their petrogenesis: Lithos, v. 34, p. 235–252.
Robin-Popieul, C.C.M., Arndt, N.T., Chauvel, C., et al., 2012, A new model for Barberton komatiites: Deep critical melting with high melt retention: Journal of Petrology. v. 53, p. 2191–2229.
Roerdink, D.L., Mason, P.R.D., Farquhar, J., and Reimer, T., 2012, Multiple sulfur isotopes in Paleoarchean barites identify an important role for microbial sulfate reduction in the early marine environment: Earth and Planetary Science Letters. v. 331, p. 177–186.
Roerdink, D.L., Mason, P.R.D., Whitehouse, M.J. and Reimer, T., 2013, High-resolution quadruple sulfur isotope analyses of 3.2 Ga pyrite from the Barberton greenstone belt in South Africa reveal distinct environmental controls on sulfide isotopic arrays: Geochimica et Cosmochimica Acta, v. 117, p. 203–215.
Roerdink, D.L., Mason, P.R.D., Whitehouse, M.J., and Brouwer, F.M., 2016, Reworking of atmospheric sulfur in a Paleoarchean hydrothermal system at Londozi, Barberton greenstone belt, Swaziland: Precambrian Research, v. 280, p.195–204.
Rudnick, R.L., and Gao, S., 2004, Composition of the continental crust, *in* Holland, H.D., and Turekian, K.K., eds., Treatise on Geochemistry, 2nd ed.: Elsevier, p. 87–118, p. 1–65.
Said, N., Kerrich, R., Cassidy, K., and Champion, D.C., 2012, Characteristics and geodynamic setting of the 2.7 Ga Yilgarn heterogeneous plume and its interaction with continental lithosphere: Evidence from komatiitic basalt and basalt geochemistry of the Eastern Goldfields Superterrane: Australian Journal of Earth Sciences, v. 59, p. 737–763.
Sandstå, N.R., Robins, B., Furnes, H., and De Wit, M.J., 2011, The origin of large varioles in flow-banded pillow lava from the Hooggenoeg Complex, Barberton greenstone belt, South Africa: Contributions to Mineralogy and Petrology, v. 162, p. 365–377.
Schneider, K.P., Hoffmann, J.E., Münker, C., et al., 2019, Petrogenetic evolution of metabasalts and metakomatiites of the lower Onverwacht Group, Barberton greenstone belt (South Africa): Chemical Geology, v. 511, p. 152–177.
Schwarz-Schampera, U., Terblanche, H., and Oberthür, T., 2010, Volcanic-hosted massive sulfide deposits in the Murchison greenstone belt, South Africa: Mineralium Deposita, v. 45, p. 113–145.
Shao, Y., Yan, D., Qiu, L., Mu, H., and Zhang, Y., 2022, Late Permian high-Ti and low-Ti basalts in the Songpan-Ganzi Terrane: Continental breakup of the western margin of the South China block: Minerals, v. 12, article 1391.
Sharman, E.R., Taylor, B.E., Minarik, W.G., Dubé, B., and Wing, B.A., 2015, Sulfur isotope and trace element data from ore sulfides in the Noranda district (Abitibi, Canada): Implications for volcanogenic massive sulfide deposit genesis: Mineralium Deposita, v. 50, p. 591–606.
Shervais, J.W., 1982, Ti-V plots and the petrogenesis of modern and ophiolitic lavas: Earth and Planetary Science Letters, v. 59, p. 101–118.
Sigmarsson, O., Hémond, C., Condomines, M., Fourcade, S., and Oskarsson, N., 1991, Origin of silicic magma in Iceland revealed by Th isotopes: Geology, v. 19, p. 621–624.
Sigmarsson, O., Condomines, M., and Fourcade, S., 1992, A detailed Th, Sr and O isotope study of Hekla: Differentiation processes in an Icelandic volcano: Contributions to Mineralogy and Petrology, v. 112, p. 20–34.
Sigurdsson, H., and Sparks, R.S.J., 1981, Petrology of rhyolitic and mixed magma ejecta from the 1875 eruption of Askja, Iceland: Journal of Petrology, v. 22, p. 41–84.
Smart, K.A., Tappe, S., Stern, R.A., Webb, S.J., and Ashwal, L.D., 2016, Early Archaean tectonics and mantle redox recorded in Witwatersrand diamonds: Nature Geoscience, v. 9, p. 255–259.
Smithies, R.H., 2002, Archaean boninite-like rocks in an intracratonic setting: Earth and Planetary Science Letters, v. 197, p. 19–34.
Smithies, R.H., Champion, D.C., and Sun, S.S., 2004, The case for Archaean boninites: Contributions to Mineralogy and Petrology, v. 147, p. 705–721.
Smithies, R.H., Champion, D.C., Van Kranendonk, M.J., Howard, H.M., and Hickman, A.H., 2005a, Modern-style subduction processes in the Mesoarchaean: Geochemical evidence from the 3.12 Ga Whundo intra-oceanic arc: Earth and Planetary Science Letters, v. 23, p. 221–237.
Smithies, R.H., Van Kranendonk, M.J., and Champion, D.C., 2005b, It started with a plume: Early Archaean basaltic proto-continental crust: Earth and Planetary Science Letters, v. 238, p. 284–297.
Spooner, E.T.C., and Fyfe, W.S., 1973, Sub-seafloor metamorphism, heat and mass transfer: Contributions to Mineralogy and Petrology, v. 42, p. 287–304.
Spulber, S.D., and Rutherford, M.J., 1983, The origin of rhyolite and plagiogranite in oceanic crust: An experimental study: Journal of Petrology, v. 24, p. 1–25.
Stein, H.J., 2014, Dating and tracing the history of ore formation, *in* Holland, H.D., and Turekian, K.K., eds., Treatise on Geochemistry, 2nd ed.: Elsevier, v. 13, p. 87–118.
Stein, H.J., and Hannah, J.L., 2015, Rhenium-osmium geochronology: Sulfides, shales, oils, and mantle: Encyclopedia of Scientific Dating Methods, p. 707–723.
Stern, R.J., Reagan, M., Ishizuka, O., Ohara, Y., and Whattam, S., 2012, To understand subduction initiation, study forearc crust: To understand forearc crust, study ophiolites: Lithosphere, v. 4, p. 469–483.
Sun, S.S., and McDonough, W.F., 1989, Chemical and isotopic systematics of oceanic basalts: Implications for mantle composition and processes: Geological Society of London, Special Publication 42, p. 313–345.
Tarduno, J.A., Cottrell, R.D., Watkeys, M.K., et al., 2010, Geodynamo, solar wind, and magnetopause 3.4 to 3.45 billion years ago: Science, v. 327, p. 1238–1240.
Tappe, S., Ngwenya, N. S., Stracke, A., et al., 2023, Plume-lithosphere interactions and LIP-triggered climate crises constrained by the origin of Karoo lamproites: Geochimica et Cosmochimica Acta, v. 350, p. 87–105.
Thy, P., Beard, J.S., and Lofgren, G.E., 1990, Experimental constraints on the origin of Icelandic rhyolites: The Journal of Geology, v. 98, p. 417–421.
Turner, S., Rushmer, T., Reagan, M., and Moyen, J.-F., 2014, Heading down early on? Start of subduction on Earth: Geology, v. 42, p. 139–142.
Van Acken, D., Hoffmann, J.E., Schorscher, J.H.D., et al., 2016, Formation of high-Al komatiites from the Mesoarchean Quebra Osso Group, Minas Gerais, Brazil: Trace elements, HSE systematics and Os isotopic signatures: Chemical Geology, v. 422, p. 108–121.
Van Kranendonk, M.J., Philippot, P., Lepot, K., Bodorkos, S., and Pirajno, F., 2008, Geological setting of Earth's oldest fossils in the ca. 3.5 Ga Dresser Formation, Pilbara craton, Western Australia: Precambrian Research, v. 167, p. 93–124.
Vermeesch, P., 2018, IsoplotR: A free and open toolbox for geochronology: Geoscience Frontiers, v. 9, p. 1479–1493.
Versfeld, J.A., 1988, The geology of the Nondweni greenstone belt, Natal: Ph.D. thesis, Durban, South Africa, University of Natal, 400 p.
Versfeld, J.A., and Wilson, A.H., 1992, Nondweni Group, *in* Johnson, M.R., ed., Catalogue of South African stratigraphic units: South African Commission for Stratigraphy, v. 4, p. 19–20.

Downloaded from http://pubs.geoscienceworld.org/segweb/economicgeology/article-pdf/120/4/903/7306681/5162_netshidzivhe_et_al.pdf
by The Lib. East China Geol Inst. user

Viljoen, M., and Viljoen, R., 1969, The effects of metamorphism and serpentinization on the volcanic and associated rocks of the Barberton region: Geological Society of South Africa, Special Publication 2, p. 29–54.
Virtanen, V.J., Heinonen, J.S., Molnár, F., et al., 2021, Fluids as primary carriers of sulfur and copper in magmatic assimilation: Nature Communications, v. 12, article 6609.
Walters, J.B., Cruz-Uribe, A.M., and Marschall, H.R., 2019, Isotopic compositions of sulfides in exhumed high-pressure terranes: Implications for sulfur cycling in subduction zones: Geochemistry, Geophysics, Geosystems, v. 20, p. 3347–3374.
Wilson, A.H., 2002, Early Archaean highly-depleted ultramafic boninitic lavas in the southern Kaapvaal craton, South Africa: Goldschmidt Conference Abstracts, v. 12, p. A839
——2003, A new class of silica enriched, highly depleted komatiites in the southern Kaapvaal craton, South Africa: Precambrian Research, v. 127, p. 125–141.
——2019, The Late Paleoarchean ultra-depleted Commondale komatiites: Earth's hottest lavas and consequences for eruption: Journal of Petrology, v. 60, p. 1575–1620.
Wilson, A.H., and Carlson, R.W., 1989, A Sm-Nd and Pb isotopic study of Archaean greenstone belts in the southern Kaapvaal craton, South Africa: Earth and Planetary Science Letters, v. 96, p. 89–105.
Wilson, A.H., and Versfeld, J.A., 1992a, Magongolozi Formation, *in* Johnson, M.R., ed., Catalogue of South African stratigraphic units: South African Commission for Stratigraphy, v. 4, p. 7–9.
——1992b, Witkop Formation, *in* Johnson, M.R., ed., Catalogue of South African stratigraphic units: South African Commission for Stratigraphy, v. 4, p. 35–37.
——1994a, The early Archaean Nondweni greenstone belt, southern Kaapvaal craton, South Africa, Part I. Stratigraphy, sedimentology, mineralization and depositional environment: Precambrian Research, v. 67, p. 243–276.
——1994b, The early Archaean Nondweni greenstone belt, southern Kaapvaal craton, South Africa, Part II. Characteristics of the volcanic rocks and constraints on magma genesis: Precambrian Research, v. 67, p. 277–320.
Wilson, A., and Riganti, A., 2022, Architectural and compositional diversity of early Earth ocean floor evidenced by the Paleoarchean Nondweni greenstone belt, South Africa: Journal of Petrology, v. 63, p. 1–32.
Wilson, A.H., Versfeld, J.A., and Hunter, D.R., 1989, Emplacement, crystallization and alteration of spinifex-textured komatiitic basalt flows in the Archaean Nondweni greenstone belt, southern Kaapvaal craton, South Africa: Contributions to Mineralogy and Petrology, v. 101, p. 301–317.
Winchester, J.A., and Floyd, P.A., 1977, Geochemical discrimination of different magma series and their differentiation products using immobile elements: Chemical Geology, v. 20, p. 325–343.
Wyman, D., and Kerrich, R., 2009, Plume and arc magmatism in the Abitibi subprovince: Implications for the origin of Archean continental lithospheric mantle: Precambrian Research, v. 168, p. 4–22.
Xie, H., Hofmann, A., Hegner, E., et al., 2012, Zircon SHRIMP dating confirms a Palaeoarchaean supracrustal terrain in the southeastern Kaapvaal craton, southern Africa: Gondwana Research, v. 21, p. 818–828.
Xie, Q., Kerrich, R., and Fan, J., 1993, HFSE/REE fractionations recorded in three komatiite-basalt sequences, Archean Abitibi greenstone belt: Implications for multiple plume sources and depths: Geochimica et Cosmochimica Acta, v. 57, p. 4111–4118.
Zhang, Q.Q., Gao, X.Y., and Zheng, Y.F., 2022, Response of trace elements to partial melting of felsic crust at high to ultrahigh temperatures: Implications for granite geochemistry: Lithos, v. 422, article 106743.
Zierenberg, R.A., Schiffman, P., Barfod, G.H., et al., 2013, Composition and origin of rhyolite melt intersected by drilling in the Krafla geothermal field, Iceland: Contributions to Mineralogy and Petrology, v. 165, p. 327–347.

Thendo Netshidzivhe is a lecturer in igneous petrology at North-West University in South Africa. She recently graduated with a PhD in geology from the University of Johannesburg specializing in komatiites and volcanogenic massive sulfide (VMS) deposits in Archean greenstone belts on the southeastern Kaapvaal craton. As she transitions into her full-time role in academia, her current research interests focus on magmatic and tectonic processes that influenced mineral deposit formation on the Kaapvaal craton.

Sebastian Tappe is a professor of economic geology and petrology at the Technical University Bergakademie Freiberg in Germany. Prior to this very recent appointment, he held faculty positions in these disciplines at the University of Johannesburg and at UiT, The Arctic University of Norway. He also had industry stints with De Beers Exploration in Toronto and Johannesburg as a specialist in petrology and geochemistry. Sebastian is interested in a range of magmatic and magmatic-hydrothermal mineralization types, ranging from primary diamond deposits through Li pegmatites to base metal sulfide deposits. His current research focuses on the geodynamic evolution and petrology of critical metal-endowed carbonatites worldwide.

Downloaded from http://pubs.geoscienceworld.org/segweb/economicgeology/article-pdf/120/4/903/7306681/5162_netshidzivhe_et_al.pdf
by The Lib. East China Geol Inst. user